Ore Geology Reviews 75 (2016) 268–283

Contents lists available at ScienceDirect

Ore Geology Reviews

journal homepage: www.elsevier.com/locate/oregeorev

# Genesis of the Saishitang skarn type copper deposit, West Qinling, Qinghai Province: Evidence from fluid inclusions and stable isotopes

Yingchuan Lu [a,b,*], Jiajun Liu [a,*], Dong Zhang [b], Emmanuel John M. Carranza [c], Degao Zhai [a], Liangsheng Ge [b], Hao Sun [b], Bin Wang [b], Yongfu Chen [b], Peng Liu [b]

[a] State Key Laboratory of Geological Processes and Mineral Resources, and School of Earth Science and Resources, China University of Geosciences, Beijing 100083, China
[b] Gold Geological Institute of CAPF, Langfang 065000, China
[c] James Cook University, Townsville 4811, Queensland, Australia

ARTICLE INFO

*Article history:*
Received 5 April 2015
Received in revised form 11 December 2015
Accepted 25 December 2015
Available online 31 December 2015

*Keywords:*
Fluid inclusion
Stable isotope
West Qinling
Saishitang copper deposit

ABSTRACT

The Saishitang skarn type copper deposit, located in the southeast part of the Dulan–Ela Mountain Triassic volcanic–magmatic arc and forearc accretionary wedge, belongs to the Tongyugou–Saishitang tin–copper polymetallic ore field in West Qinling, Qinghai province. Based on the contact/crosscutting relationships, mineral associations and mineralization characteristics, hydrothermal fluid evolution can be divided into three stages: skarn (I), quartz sulfide (II) and polymetallic sulfide-bearing quartz–calcite vein (III). The quartz sulfide stage (II) can be further divided into a massive sulfide stage (II-1) and a layered sulfide stage (II-2). This paper presents detailed analysis of fluid inclusions, H–O, S and Pb isotope compositions of rock samples from each of the above three stages as well as analysis of fluid inclusions from quartz diorite. The homogenization temperature, salinity, density and pressure of fluid inclusions in quartz diorite and typical transparent minerals showed a tendency of gradual decline in these evolutionary stages. The ore-forming fluid can be classified as a $Na^+$–$Ca^{2+}$–$SO_4^{2-}$–$Cl^-$ system with a minor proportion of a $Na^+$–$Ca^{2+}$–$NO_3^-$ $SO_4^{2-}$ system, which likely resulted from mixing of magmatic and formation water. The H–O isotope composition indicates that the proportion of formation water increased during the ore-forming process, and meteoric water was mixed in the late quartz–calcite vein stage. The $\delta^{34}S$ (CDT) values (−6.45–5.57‰) and Pb isotope compositions show that the ore-forming materials were mainly derived from magmatic fluid. Ore-forming fluid was boiling during the main ore-forming stage (II-1) due to pressure decrease. Consequently, the physical and chemical conditions (i.e., pH, Eh, $f_{O2}$, $f_{S2}$) changed, and metallic elements (including Cu) in the fluid could no longer exist in the form of complexes and precipitated from the fluid. According to the integrated analysis of ore features, mineral associations, alteration characteristics, ore-forming environment and fluid evolutionary process, it is concluded that the Saishitang deposit is a typical skarn deposit.



## 1. Introduction

The Qinling orogenic belt (QOB), which is a composite continental orogenic belt, is an important part of central orogenic system of mainland China (Zhang et al., 2001; Liu et al., 2015a, 2015b). The Western Qinling Mountains are the western extension of the QOB and are located between the northeastern margin of the Qinghai–Tibet Plateau and the northwestern margins of the Yangtze Plate, South Qilian Mountains and East Kunlun Mountains (Zhang et al., 2004). They form the western Qinling orogenic belt (WQOB) in the Qinling–Qilian–Kunlun metallogenic domain, which provides nonferrous and precious metal resources to Qinghai Province.

Situated on the western margin of the WQOB is the Tongyugou–Saishitang copper–polymetallic ore field. This ore field, which is one of the most important regions of copper resources in Qinghai or even in China (Song et al., 1995; Liu et al., 2008a), is comprised of the large-scale Tongyugou copper deposit (a total resource of more than 500,000 tons), the medium-scale Saishitang copper deposit (a total resource of 444.8 thousand tons) (Liu et al., 2008b), the Rilonggou stannous-polymetallic ore deposit, the Gakehe copper–silver–arsenic occurrence and the Lajiehai molybdenum–copper occurrence. These deposits, particularly the Saishitang, have distinct geological and geochemical features compared to other large-scale skarn deposits in the WQOB, and represent a specific type of mineralization that is rarely reported in western literature.

Due to the diversity and distinctiveness of ore types in the Saishitang ore field, there is no consensus among previous researchers (Qiu and Dong, 1978; Lin, 1983; Lu, 1990a; Li et al., 1993; Tian, 1999 and Wu, 2010) regarding the genesis of the Saishitang copper deposit.

* Corresponding authors at: State Key Laboratory of Geological Processes and Mineral Resources, China University of Geosciences, Beijing 100083, China.
*E-mail addresses:* luyingchuan2008@163.com (Y. Lu), liujiajun@cugb.edu.cn (J. Liu).

http://dx.doi.org/10.1016/j.oregeorev.2015.12.020
0169-1368/

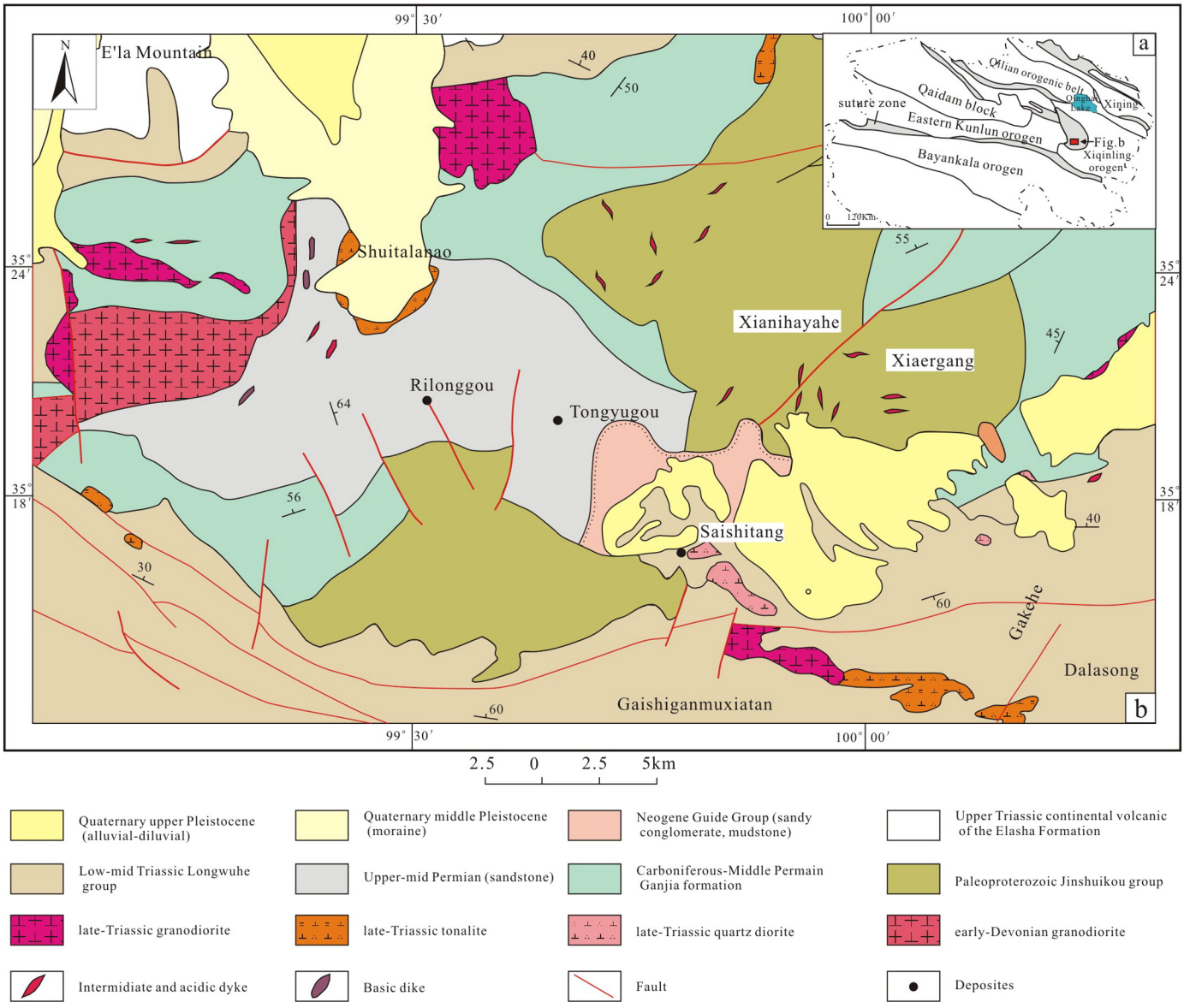


**Fig. 1.** Sketch geological map of Saishitang copper deposit (a — after (Zhang and Yang, 2007); b — after Li et al., 2009).

Strata-bound-, skarn- and porphyry-type styles of mineralization have been proposed for this deposit. Despite the volume of research spent on this deposit, the fluid inclusion aspect of the deposit, which is critical to a comprehensive understanding of ore genesis, is much less studied. The characteristics of ore-forming fluid provide important clues for understanding the genesis of ore deposits (e.g., Zhu et al., 2001; Fan et al., 2003; Xu et al., 2006). Therefore, it is necessary to consider in more detail the origin and evolution of hydrothermal fluids responsible for the Saishitang copper deposit.

In this paper, we discuss results of geological investigations, ore microscopy, fluid inclusion micro-thermometry, O–H and S isotope measurements, which help to clarify the ore genesis of the Saishitang Cu deposit. We also discuss the P–T conditions during mineral–fluid evolution of the Saishitang Cu deposit based on fluid inclusion data to further constrain the fluid origin of the deposit.

## 2. Geological background

The Saishitang copper–polymetallic ore deposit is located in the Dulan–E'la Mountain Triassic volcanic–magmatic arc and the southeast part of the fore-arc accretionary wedge (Wu, 2010). This is the junction between the WQOB and the Eastern Kunlun orogenic belt (Fig. 1a). The Carboniferous–Early Permian was once the northern branch of eastern Kunlun Ocean, with collision and extrusion occurring in east–west direction in early Triassic. Late Triassic adakite magmatism occurred in this region along the middle Kunlun fault (Zhang and Zhu, 2001). Rock-controlling and ore-controlling characteristics are shown to be composite tectonic features with east-to-west and northwest trends (Zhan et al., 2007).

The lithologies of the WQOB consist of the Paleoproterozoic Jinshuikou Group, the Carboniferous–Middle Permian Ganjia Group, the Lower–Middle Triassic Longwuhe Group, continental volcanic rocks of the Upper Triassic E'la Mountain Group, red glutenite of the Neogene Guide Group, mudstone, Pleistocene moraine of the Quaternary system and Upper Epipleistocene proluvium. The Ganjia Group is a sequence composed of a combination of clastic and carbonate rocks. The Longwuhe Group is composed of gray feldspar–quartz metamorphic rock, silty and clay slate, and bedded gravel-bearing feldspar lithic sandstone.

Faults with NW, E–W trending, and occasionally NE and nearly N–S trends are the dominant tectonic structures in the region. The E–W and NW-trending faults are closely associated with the mineralization. Four

types of folding were developed. The first type is recumbent folding, developed in the Proterozoic block. The second type is folding (type-A fold) associated with thrusting and strike–slip shearing, and is developed in the strong deformation zone and shows features of shallow tectonic levels. The third type is overturned folding with same inclination developed in the thrust fault–fold belt. The fourth type is folding with N–NW trends is multi-hinge and high-angle pitch. Stage four folds consist of the Xueqinggou anticlinorium, the Saishitang anticline, the Tongyugou short-axis anticline, and the Rilonggou anticline.

The magmatic rocks in this region can be divided into four categories: (1) diorite porphyrite; (2) quartz diorite (221.7 ± 2.8 Ma, unpublished result), quartz diorite porphyrite (223.2 ± 2.2 Ma; Liu et al., 2012); (3) plagiogranite porphyry; (4) granitic porphyry (219 ± 2.6 Ma; Liu et al., 2012), quartz porphyry and fine-grained granite. The second category of intrusions represents the largest scale of igneous activity and resulted in the emplacement of quartz–diorite, which represents the bulk of the Saishitang composite rock mass. This rock is fine-grained hypautomorphic granular texture with a blocky structure, and pervasive sericitization and chloritization (Lai et al., 2010).

## 3. Ore deposit geology

The rock units in the Saishitang ore field consist of Lower Permian and Tertiary lithologies and Quaternary loose or semi-consolidated deposits. The Lower Permian series is the main ore-bearing strata consisting of the fifth, sixth and seventh lithologic units of the formation. The fifth lithologic unit is medium to thick layer of gray metamorphosed fine-grained feldspathic quartz sandstone interbedded with sericite phyllite. The sixth lithologic unit is off-white metamorphosed fine-grained feldspathic quartz sandstone, metamorphosed fine-grained quartz sandstone and sericite phyllite. The seventh lithologic unit is off-white banded metamorphosed siltstone, biotite phyllite, marble, and off-white marble interbedded with skarn (Fig. 2a).

Multiple faults with E–W, WNW, NNW and NE trends are present in the Saishitang ore field. Some rock-controlling and ore-controlling structures are associated with folds. Fold activity was dominated by compression-shear and partly by tension-shear. Folds are among the most important structural features in the Saishitang ore field, and they can be divided into (1) tight homoclinal folds; (2) NW–NNW-trending Alpine-style tight linear folds; (3) nearly NE-trending folds and (4) NNE–NE-trending folds. The interlayer detachment zone or detachment fault zone related to (1) and (2) types of folds are the most important rock-controlling and ore-controlling structures during the metallogenic period (Zhu et al., 2012).

Quartz diorite (with the U–Pb age of 221.7 ± 2.8 Ma, unpublished result) is the main intrusive rock in the Saishitang ore field, followed by quartz diorite porphyry, quartz porphyry and dacite porphyry. It generally occurs as sheet-like and bed-like shape, and some are in apophysis and veins. It is fine- and medium-grained type, and the medium-grained quartz diorite commonly intrudes into the fine-grained quartz diorite, with the existence of xenolith of the latter in the former.

The immediate host to ore bodies in the Saishitang ore field is the quartz diorite (Tian, 1999; Li et al., 2009), which occurs as sills (~500 m-thick), dykes (~50 m-thick) and dykelets (~20 m-thick). The quartz diorite typically shows a porphyritic texture, and primary minerals include plagioclase (~20 vol.%), hornblende (~15 vol.%), quartz (~5 vol.%), biotite (~5 vol.%) and minor microcline. Plagioclase phenocrysts are commonly tabular in shape, and display rhythmic zonings and polysynthetic twinnings. They have been mainly overprinted by sericite (Fig. 3e), and occasionally by chlorite and epidote. Hornblende has been replaced by epidote (Fig. 3f). Sulfide minerals including bornite (<5 vol.%), pyrite(<3 vol.%) and chalcopyrite (<1 vol.%) are also present in the intensely-altered quartz diorite (Fig. 3h and i).

The ore bodies mainly exist in the skarn contact zone between quartz diorite and marble (Fig. 2b). The ore-bearing porphyry has experienced complete alteration, with an increase of copper content in the rock from the ore-bearing rock outwards to the contact zone. Beyond the contact zone the copper content decreases gradually (Li et al., 2009). By detailed geological survey, ore exploration and documentation, the contact or alteration relationship of rocks, mineral assemblage and mineralization characteristics were summarized. The evolution of ore-forming process was divided into three stages: (I) magmatic (quartz diorite) skarn stage; (II) quartz–sulfide stage; and (III) late sulfide-bearing quartz–carbonate vein stage. The quartz–sulfide stage was subdivided into massive sulfide stage (II-1) and layered metal sulfide rock stage (II-2).

In the quartz diorite bodies, no mineralization occurred in the skarn stage (I). The main skarn minerals are garnet (about 35%), clinopyroxene (about 30%) and vesuvianite (about 25%). Skarns near the quartz diorite intrusion are garnet-rich, with garnets being either tightly packed together or fine- to medium-grained (Fig. 3g). Tightly packed garnets always coexist with clinopyroxene, the former being located closer to the intrusive body. Partial replacement of garnet by vesuvianite (Fig. 3g) shows that garnet formed earlier than vesuvianite. Fine- to medium-grained clinopyroxenes, some of which have quartz-filled crystal gaps, do not co-exist with garnets (Fig. 3h).

Rocks associated with stages II-1 and II-2 are either massive (Fig. 3b) or layered (Fig. 3c). Ores are dominated by chalcopyrite, bornite, pyrite and sphalerite. Replacement of nonmetallic mineral by bornite indicates that the latter formed later than the former (Fig. 3i). Chalcopyrite usually coexists with bornite (Fig. 3j), and both minerals are separated from the solid solution of chalcopyrite and sphalerite (Fig. 3k). Gangue minerals are mainly quartz, tremolite and fluorite. Polymetallic sulfide-bearing quartz–calcite veins (stage III) filled fractures (Fig. 3d), with associated pyrite, chalcopyrite and bornite (Fig. 3l).

## 4. Analysis of fluid inclusions

### 4.1. Sampling and analytical method

Samples of quartz diorite were collected from the Saishitang ore field (sample No.: 12SST-09-1, 12SST-20 and 12SST-27). Samples were also collected from skarn stage (I: 12SST-26, 12SST-28), quartz-sulfide stage (massive copper ore, II-1, 12SST-12; layered copper ore, II-2, 12SST-21) and late sulfide-bearing quartz–calcite vein stage III, 12SST-24, 12SST-25). From each of these stages of ore-forming process, the most representative minerals were sampled for analysis. The specific sampling locations were shown in Fig.2b. The host minerals of fluid inclusions in samples for the temperature measurement are: quartz phenocrysts, amphibole, epidote and ordinary quartz from quartz diorite; garnet, clinopyroxene, tremolite and vesuvianite from stage I; quartz from stage II-1; quartz, fluorite and clinopyroxene from stage II-2, and quartz from stage III. These different mineral assemblages reflect diverse hydrothermal environments. Quartz phenocrysts and amphibole in quartz diorite reflect the temperature during condensation of magmatic hydrothermal fluid. The features of the samples are listed in Fig. 3.

Temperature measurements from fluid inclusions were carried out at the fluid inclusion laboratory in China University of Geosciences Beijing. The Linkam THMSE-600 (Linkam, England) heating and freezing stage was used. The reproducibility error of measuring homogenization temperature was kept below 2 °C, while the reproducibility error of measuring freezing temperature was kept below 0.2 °C. When measuring freezing temperature, liquid nitrogen was used for rapid cooling of the inclusions. Thus, the liquid phase was completely solidified, and the changes of the inclusions were observed as the temperature declined. When temperature dropped to −120 °C, the temperature was then raised slowly until the last ice crystal melted. The freezing temperature was thus measured ($t_m$) (Liu and Shen, 1999). When measuring homogenization temperature, the initial rate of temperature rise was 10 °C/min. When the phase approached the homogenized state, the

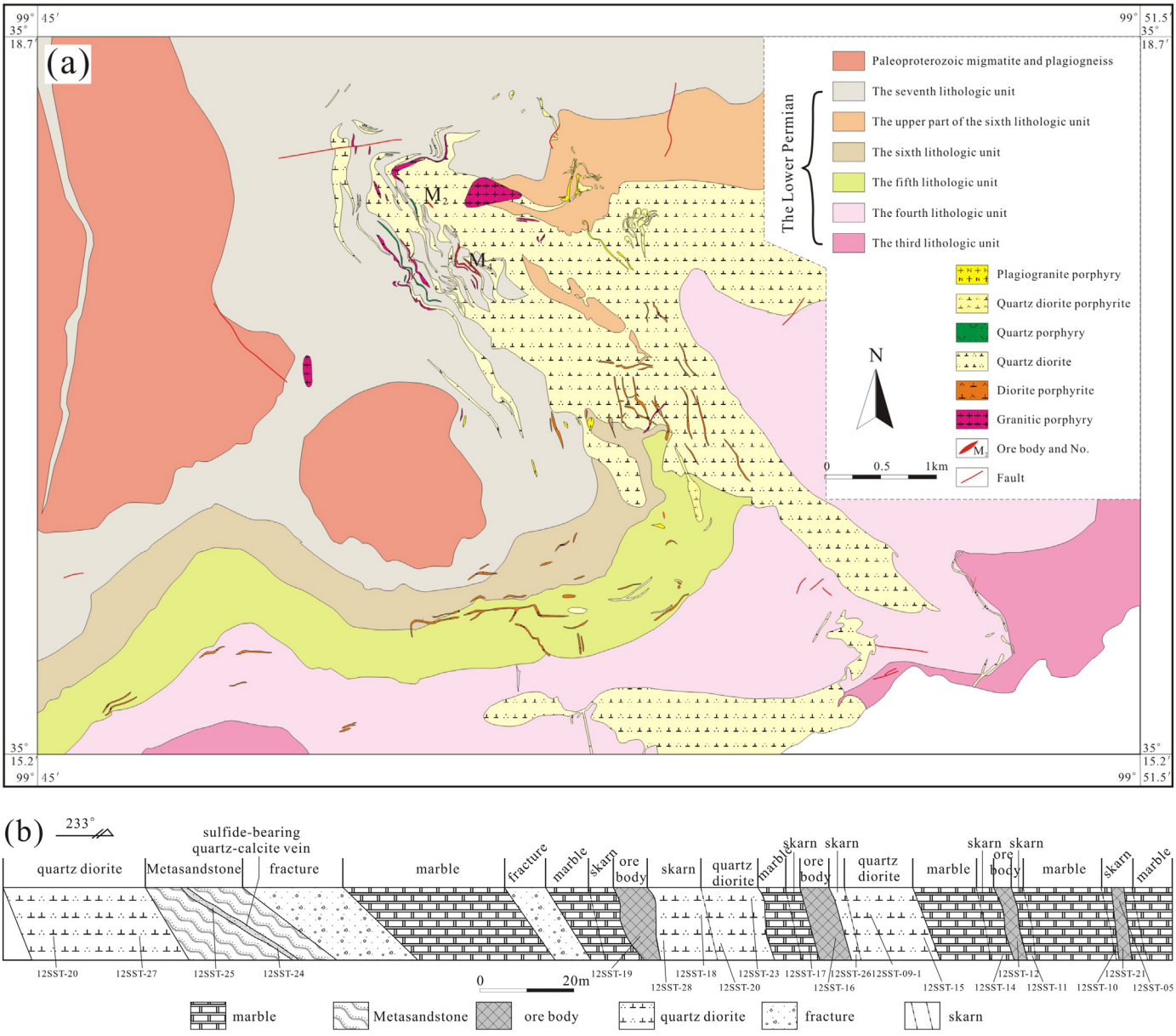


**Fig. 2.** Geological sketch map of Saishitang copper deposits (a) and the sketch map of 3350 level cross cutting in Saishitang skarn copper deposit (b).

rate of temperature rise was reduced, and the homogenization temperature was recorded timely.

For type H (multiphase inclusions containing daughter minerals) inclusions containing mineral crystals, heating was employed to determine the melting temperature of NaCl daughter minerals. The temperature corresponding to the disappearance of NaCl daughter minerals was looked up from a table in Lu et al. (2004). The salinity was determined as 28.59–6 4.47% $NaCl_{eqv}$ according to that table. The freezing method by Hall et al. (1988) was employed to determine the scope of freezing temperature. Salinity was calculated as $W = 0.00 + 1.78T_{m(ice)} + 0.0442T^2_{m(ice)} + 0.000557T^3_{m(ice)}$. Thus, the salinities of types V (vapor or gas) and L (liquid) inclusions containing no halite daughter minerals were obtained. The liquid- and gas-phase components of fluid inclusions were analyzed by the Analytical Laboratory of the CNNC Beijing Research Institute of Uranium Geology. The liquid-phase components were measured using DIONEX-500 Ion Chromatograph (serial number 6319, relative humidity 35%, temperature 22 °C). The gas-phase components were analyzed by thermal conductivity detector (TCD, PE.Clarus600), with the flow rate of carrier gas being 25 ml/min, pressure of carrier gas ($Ar_2$) 100 KPa and the room temperature of 25 °C. The decrepitation temperature was 550 °C and the decrepitation time was 5 min.

### 4.2. Petrographic analysis of fluid inclusions

The fluid inclusions studied have developed in the stages of ore-forming process from magmatic to dry skarn and wet skarn stage and finally to the sulfide-bearing hydrothermal quartz stage. Therefore, the types of fluid inclusions studied also differed with the ore-forming stages. Primary fluid inclusions were mainly studied. They exhibit various morphologies such as negative crystal, oval, rhombic, square, rectangular, trapezoidal, triangular and irregular. Their sizes vary in the range of 5–20 μm. Considering the phase of fluid inclusions and the transparent daughter minerals in fluid inclusions at room temperature (An, 2010), the fluid inclusions in the Saishitang ore field can be divided into four types:

(1) Melt inclusions (type G + W): They are composed of glass (Gl), gas bubble (G), crystalline aggregate (devitrification products) with or without one or more daughter minerals (Fig. 4a, b). They are

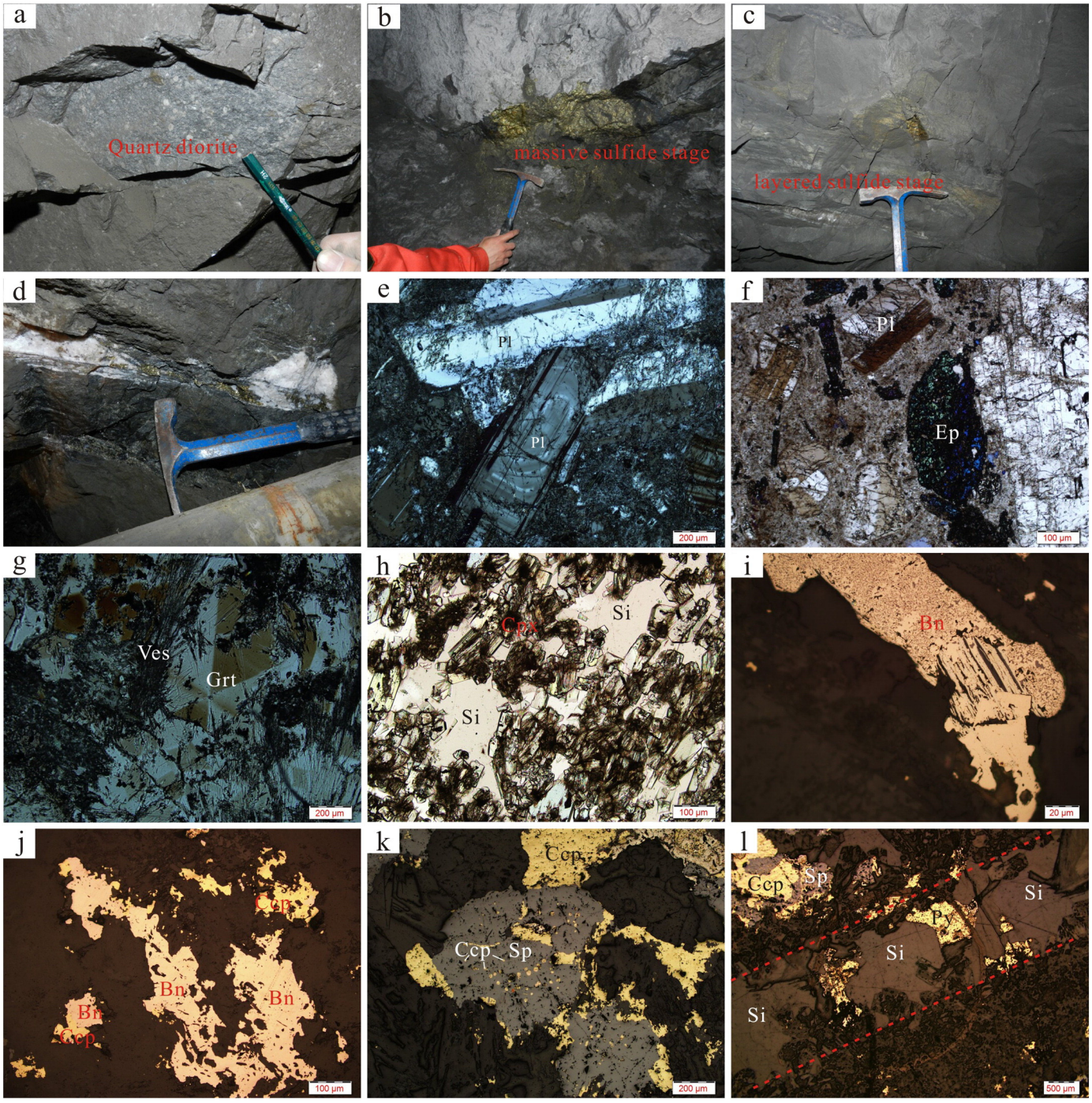


**Fig. 3.** Field photographs and photomicrographs of the studied samples. a — Quartz diorite; b — Massive skarn ore; c — Stratiform skarn ore; d — Sulfide bearing quartz calcite vein; e — Zoned plagioclase; f — Hornblende is altered to epidote; g — The garnet partial replacement by vesuvianite; h — Clinopyroxene; i — The replacement of transparent mineral by bornite; j — Chalcopyrite and bornite symbiosis; k — The chalcopyrite separation of the solid solution in sphalerite; l — The polymetallic sulfide-bearing quartz–calcite veins associated with pyrite, chalcopyrite and bornite. Bn — Bornite; Ccp — Chalcopyrite; Cpx — Clinopyroxene; Grt — Garnet; Sp — Sphalerite; Ves — Vesuvianite.

dominantly ellipsoidal and irregularly shaped, with sizes varying in the range of 10–15 μm. The gas fraction is 5–10%. With increasing temperature during heating, these inclusions became increasingly transparent and the salt minerals disappeared first. However, this type of inclusions has high homogenization temperatures (Roedder, 1992, 1994; Touret and Frezzotti, 1993), and so the glass component did not melt at the highest testing temperature of 600 °C. Although homogenization temperature was not reached, these inclusions record immiscible silicate melts and high-salt liquid trapped in the magmatic stage (Lu et al., 2004). They represent the magmatic fluid during magmatic differentiation (Lu, 1990b; Hou et al., 2013).

(2) Inclusions containing aqueous liquid of daughter minerals (type H): The sizes of this type of fluid inclusion are always <10 μm. They have amygdaloidal and columnar shapes. They contain aqueous liquid with salinity >28.59% (type W) and with one or more daughter minerals. The transparent daughter minerals are cubic and were considered as halite (Fig. 4c, d). The gas fraction was 5–40%. The gas bubbles disappeared first upon heating and then the minerals disappeared with homogenization to liquid phase for the most part. Few of the inclusions homogenized to gas phase.

(3) Gas fluid inclusions (V): Their sizes vary in the range of 5–10 μm. They have amygdaloidal and columnar shapes. They are composed of

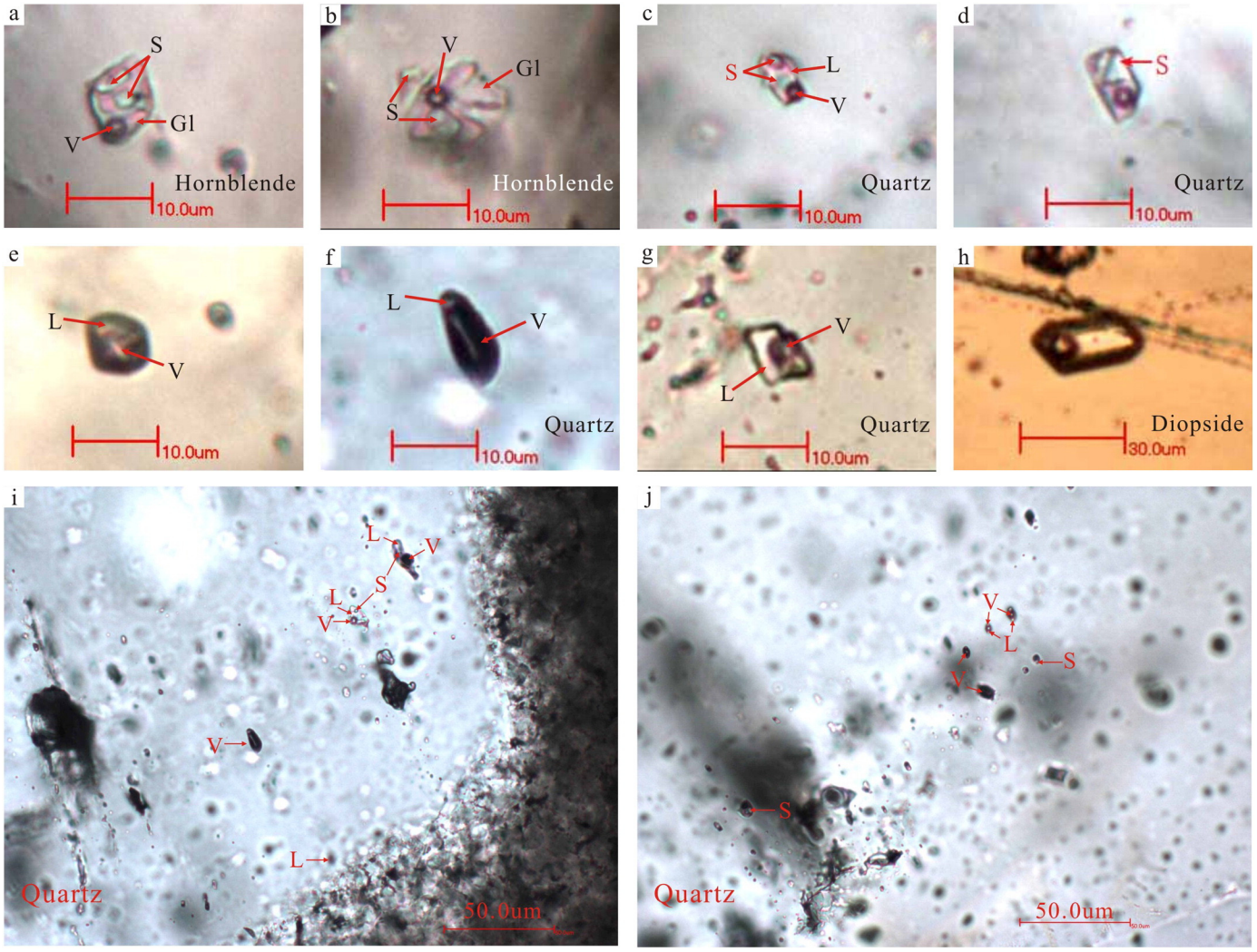


**Fig. 4.** Photomicrographs of fluid inclusions from Saishitang copper deposit a, b — Melt inclusions; c, d — Inclusions containing aqueous liquid of daughter minerals; e, f — Gas inclusions; g, h — Liquid fluid inclusion; i, j — Boiling inclusion group. Gl — glass; V — gas; L — liquid; S — daughter minerals.

liquid and gas phases, with the latter being dominant and reaching >50%. They homogenized to gas phase upon heating (Fig. 4e, f).

(4) Liquid fluid inclusions (L): These are dominated by liquid-rich low-salinity brine inclusions of various sizes (5–30 μm), various shapes (irregular, amygdaloidal and columnar) and with a range of vapor–liquid ratios (10–50%). They homogenized to liquid phase upon heating (Fig. 4g, h).

In quartz diorite closely related to skarn, amphiboles, quartz phenocrysts, ordinary quartz and epidotes all contain fluid inclusions. Amphiboles mainly have melt inclusions (G + W). Quartz phenocrysts have developed daughter mineral inclusions (type H), gas inclusions (type V) and fluid inclusions (type L), with a few melt inclusions. Ordinary quartz has two-phase gas–liquid aqueous inclusions (V + L). Fluid inclusions (type L) in epidotes are mainly developed in late alteration stage. In the samples of skarn stage (I), garnets, clinopyroxenes and vesuvianites are the representative minerals with fluid inclusions. Garnets have types H, V and L inclusions. Clinopyroxenes and vesuvianites have types H and type L inclusions. From samples of massive skarn-type copper ore belonging to the quartz–sulfide stage (II-1), fluid inclusions (types H, V and L) in quartz were chosen for the research. Quartz, fluorite and diopside are developed in skarn-type copper ore (stage II-2), and contain dominant fluid (type L) inclusions. Type L fluid inclusions are developed in quartz in late quartz–sulfide stage (III). Judging from the minerals with fluid inclusions, G + W and type H inclusions formed in an earlier period, types V and L formed in a later period.

### 4.3. Homogenization temperature and salinity of inclusions

The homogenization temperatures and salinities of each type of fluid inclusions from the Saishitang ore field are shown in Table 1. Melt (G + W) inclusions in quartz diorite from this ore field have homogenization temperatures with an upper bound of >600 °C and salinities of 39.43–40.61% $NaCl_{eqv}$. Type H inclusions have homogenization temperatures of 402–534 °C, and a few inclusions have >600 °C, and their salinities vary in the range of 38.63–64.47% $NaCl_{eqv}$. Type V inclusions have homogenization temperatures of 216–308 °C. Type L inclusions representing the late alteration stage have homogenization temperatures of 146–329 °C, mainly in the interval of 240–300 °C (Fig. 5a), with salinities of 3.87–6.30% $NaCl_{eqv}$.

In skarn stage (I), type H inclusions have complete homogenization temperatures in a wide range of 349–600 °C with salinities of 31.87–61.27% $NaCl_{eqv}$. Only one type V inclusion was found, and it has homogenization temperature of >600 °C. Type L inclusions have the lowest homogenization temperatures, which are 264–375 °C, and their salinities are 9.86–12.51% $NaCl_{eqv}$.

xIn the massive sulfide stage (II-1), type H inclusions have homogenization temperatures of 205–341 °C and salinities of 28.59–41.58% $NaCl_{eqv}$. Only two type V inclusions were found, and their homogenization temperatures are 358 °C and 360 °C. Type L inclusions have homogenization temperatures of 262–358 °C and salinities of 17.87–21.11% $NaCl_{eqv}$. In the layered copper ore stage (II-2), only type L inclusions

**Table 1**
Microthermometric results of fluid inclusions from Saishitang copper deposit.

| Stage | Type (number) | Mineral | Size (μm) | Gas fraction | $t_{bubble}$/°C | $t_m$/°C | $t_{ice}$/°C | $t_h$/°C | w (NaCleqv)% | Density (ρ) g/cm$^3$ | Pressure (P) MPa | Note |
|---|---|---|---|---|---|---|---|---|---|---|---|---|
| quartz diorite | G + W (4) | Amphibole and quartz phenocrysts | 5–13 | 5–10 | 142–206 | 316–320 | | >600 | 39.43–40.61 | 1.11–1.30 | 3.12–8.90 | Most of the daughter minerals melting temperature >600 °C |
| | H (15) | Amphibole and quartz phenocrysts | 5–12 | 10–40 | 160–305 | 329–534 | | 402–534 | 38.63–64.47 | 0.52–1.24 | 2.70–5.71 | Some of the daughter minerals melting temperature 600 °C |
| | V (5) | Quartz phenocrysts and | 3–7 | 50–60 | 216–308 | | −3.9–−2.3 | 216–308 | 3.87–6.30 | 0.75–0.89 | 0.21–0.93 | |
| | L (34) | Quartz phenocrysts, quartz and epidote | 3–18 | 5–40 | 146–329 | | −15.2–−1.6 | 146–329 | 2.74–18.8 | 0.75–1.35 | 0.12–1.11 | |
| I | H (27) | Garnet, clinopyroxene, vesuvianite | 3–26 | 5–30 | 256–600 | 460–511 | | 349–600 | 31.87–61.27 | 0.83–1.30 | 2.63–5.83 | Some of the daughter minerals melting temperature 600 °C |
| | V (2) | Garnet | 4 | 50 | | | | >600 | | | | One fluid inclusion |
| | L (24) | Garnet, clinopyroxene, vesuvianite | 2–17 | 10–40 | 264–375 | | −8.7–−6.5 | 264–375 | 9.86–12.51 | 0.71–0.79 | 1.23–2.04 | |
| II-1 | H (10) | Quartz | 3–19 | 5–12 | 176–298 | 120–341 | | 205–341 | 28.59–41.58 | 1.00–1.14 | 0.29–8.74 | |
| | V (2) | Quartz | 5–12 | 80, 90 | | | | 358, 360 | | | | Tow fluid inclusions |
| | L (7) | Quartz | 2–8 | 10–30 | 262–358 | | −18.2–−14.1 | 262–358 | 17.87–21.11 | 0.85–1.09 | 0.02–1.53 | |
| II-2 | L (25) | Fluorite, clinopyroxene and quartz | 5–35 | 10–30 | 186–385 | | −4.2–−0.6 | 186–385 | 1.05–6.74 | 0.78–0.89 | 0.11–1.00 | |
| III | V (1) | Quartz | 4 | 40 | | | −1.0 | 436 | 1.74 | | | One fluid inclusion |
| | L (18) | Quartz | 1–6 | 5–30 | 141–358 | | −2.6–−0.9 | 141–358 | 1.57–4.34 | 0.61–0.94 | 0.04–0.47 | |

Note: $t_{bubble}$/°C — Bubble disappear temperature; $t_m$/°C — Mineral disappear temperature; $t_{ice}$/°C — freezing point temperature; $t_h$/°C — complete homogenization temperature.
G + W: Melt inclusions; H: Inclusions containing aqueous liquid of daughter minerals; V: Gas inclusions; L: Fluid inclusion.
Continued to Table 1 Microthermometric result of fluid inclusions from Saishitang copper deposit.

were found, and they have homogenization temperatures of 186–385 °C and salinities of 1.05–6.74% $NaCl_{eqv}$.

In the late sulfide-bearing quartz–carbonate vein stage (III), one type V inclusions has homogenization temperature of 436 °C, and some type L inclusions have homogenization temperatures of 141–358 °C. Their corresponding salinities are 1.74% $NaCl_{eqv}$ and 1.57–4.34% $NaCl_{eqv}$, respectively.

As shown from the histogram of homogenization temperatures (Fig. 5) and Table 1, homogenization temperatures and salinities of fluid inclusions decreased with the stages. The homogenization temperatures of fluid inclusions in quartz diorite, skarn stage and late hydrothermal stage demonstrate a good correspondence relationship. Homogenization temperatures of G + W inclusions and type H inclusions in quartz diorite are comparable to those of type H inclusions in stage I. Homogenization temperatures of type V inclusions in quartz diorite are comparable to those in stage II-1. Homogenization temperatures of type L inclusions in quartz diorite are comparable to those in stages II-2 and III.

### 4.4. Inclusion density, pressure and mineralization depth

The empirical equation $\rho = a + bT_h + cT_h^2$ (a, b and c are dimensionless parameters, converted from salinity) derived by Liu and Duan (1987); Liu and Shen (1999); Liu (2001) was used to calculate the density of type H, V and L inclusions. By referring to the P–T phase diagram of NaCl–$H_2O$ system (Bodnar and Vityk, 1994), the pressures (homogenization pressure) of ore-forming fluids in each stage were obtained. The silicate melt in the melt inclusions has a very small compressibility, and the effect of pressure on trapping temperature is far smaller than the measurement error of homogenization temperature (Lu, 1990b). Thus, it was very difficult to obtain the pressure of melt inclusions. However, using the fluid inclusions coexisting but not immiscible with the melt inclusions, the same empirical formula used for type H, V and L inclusions $P = P_0Th/T_0$ (where $P_0 = 219 + 26.20w$, $T_0 = 374 + 9.20w$) (Shao, 1990) was used to calculate the pressure values of melt inclusions (Hou et al., 2013).

As shown in Table 1, the densities of types G + W, H, V and L inclusions are 1.11–1.30 g/cm$^3$, 0.52–1.24 g/cm$^3$, 0.75–0.89 g/cm$^3$ and 0.75–1.35 g/cm$^3$, respectively. The corresponding pressures are 3.12–8.90 MPa, 2.70–5.71 MPa, 0.21–0.93 MPa and 0.12–1.11 MPa, respectively. For the skarn stage (I), densities of types H and L inclusions are 0.83–1.30 g/cm$^3$ and 0.71–0.79 g/cm$^3$, respectively. The corresponding pressures are 2.63–5.83 MPa and 1.23–2.04 MPa, respectively. For the massive sulfide stage (II-1), densities of types H and L inclusions are 1.00–1.14 g/cm$^3$ and 0.85–1.09 g/cm$^3$, respectively. The corresponding pressures are 0.29–8.74 MPa and 0.02–1.53 MPa, respectively, suggesting a wide variation range of pressures and the phenomenon of decompression. For the layered sulfide stage (II-2), densities of type L inclusions are 0.78–0.89 g/cm$^3$, corresponding to pressures of 0.11–1.00 MPa. For the late sulfide-bearing quartz–calcite vein stage (III), densities are 0.61–0.94 g/cm$^3$, corresponding to the lowest pressures of 0.04–0.47 MPa.

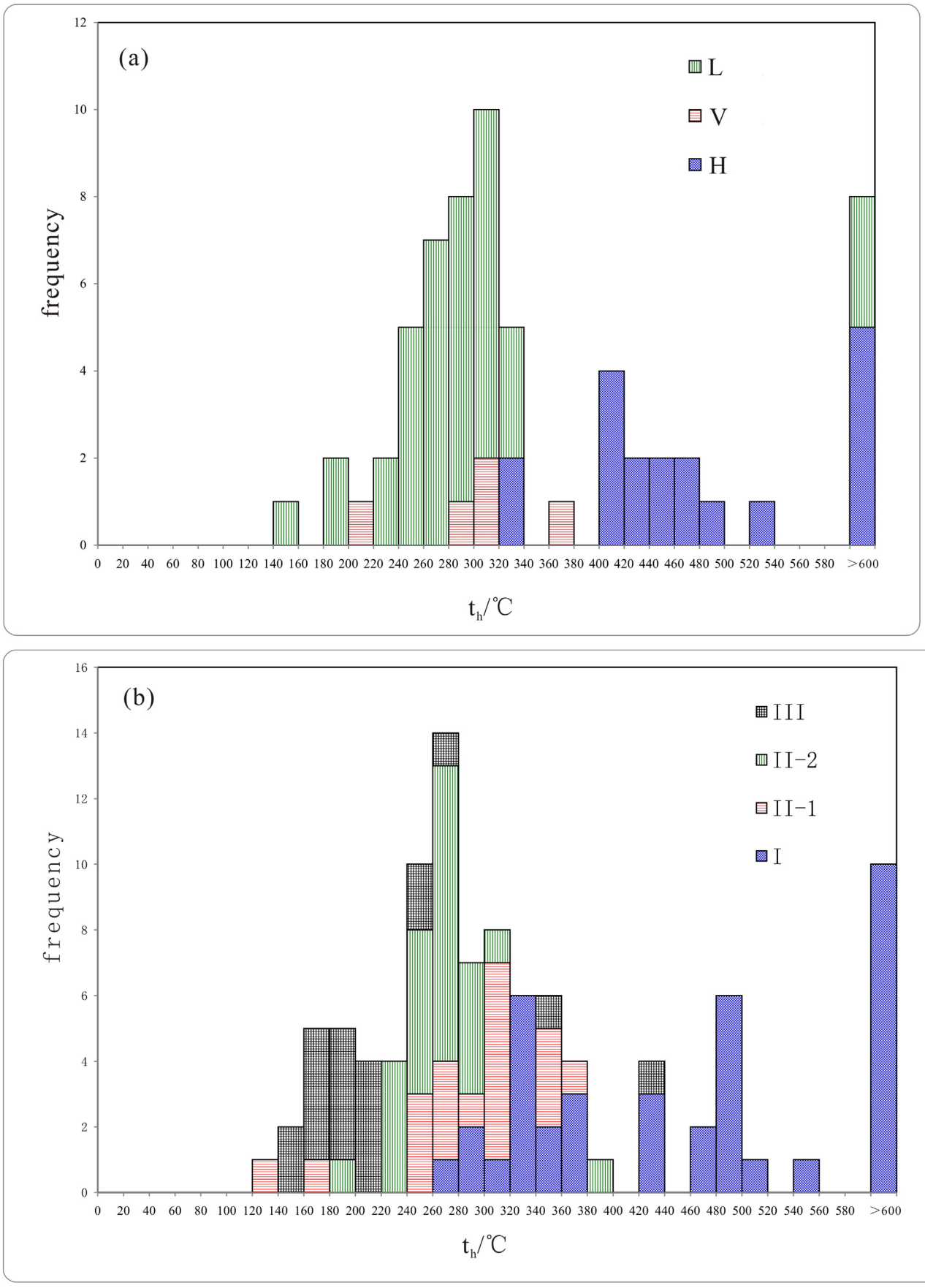


**Fig. 5.** Homogenization temperatures of fluid inclusions from Saishitang copper deposit. a — Quartz diorite period; b — skarn stage (I), quartz sulfide stage (II; massive sulfide stage (II-1), layered sulfide stage (II-2)) and polymetallic sulfide-bearing quartz–calcite vein stage (III) (The data points from different mineralization periods).

The mineralization depth of fluid was estimated from the calculated trapping pressures of fluid inclusions. Given the temperature and salinity of a boiling inclusion assemblage, the pressure during the formation of ore deposits could be estimated precisely (Roedder and Bodnar, 1980). For the massive sulfide stage of wet skarn (stage II-1), fluid boiling is highly probable (Fig. 3i, j) as indicated by alternating lithostatic and hydrostatic pressures of fluid (Li et al., 2007). The solubility curve of NaCl in saturated gas of the $H_2O$–NaCl system and the Pressure–Volume–Temperature–position (PVTx) data of liquid–gas interface were obtained by experiments and theory. The composition and trapping pressure were obtained with reasonable precision and accuracy through the study of fluid inclusions (1) where the daughter minerals disappeared first and gas bubbles disappeared next and (2) where the daughter minerals and gas bubbles disappeared simultaneously ($T_m = Th$). For fluid inclusions (3) where the gas bubbles disappeared first and the daughter minerals disappeared next ($T_m > Th$), there was a lack of liquidus line of NaCl and the PVTx data of the liquid–NaCl stability region fall outside the 40 wt.% NaCl system. Therefore, it was impossible to estimate reliably the composition and homogenization pressure of inclusions according to micro-thermometric data (Zhang et al., 2011). Thus, the pressure values of inclusions (3) were not used for the calculation of mineralization depth. Instead, the pressures of inclusions (1) and (2) trapped in the same mineral were used to calculate the paleodepth of trapping.

According to the calculation, type G + W inclusions and types H and W inclusions have strongly different pressures. This was considered as the indicator of the lithostatic or hydrostatic state of the ore-forming fluids (Hou et al., 2013). The high-pressure inclusions were treated as belonging to lithostatic system while the low-pressure inclusions as fluid belonging to hydrostatic system. These inclusions correspond to different fluid types at different stages of ore-forming process. The magmatic fluid was subject to lithostatic pressure while the ordinary fluid to hydrostatic pressure. The general expression of the relationship between pressure and depth is $P = H\rho g$. When under lithostatic pressure, the value of ρ was taken as the average rock density of mainland China, which is 2.7 g/cm$^3$; when under hydrostatic pressure, the value of ρ was calculated separately for each type of inclusion. Thus, the calculated paleodepths of trapping are as follows: depth of quartz diorite intrusion 4.2–10.0 km; depth at stage I 4.2–10.5 km; depth at stage II-1 3.1–9.8 km; depth at stage II-2 1.2–6.4 km; depth at stage III 0.3–6.0 km. Therefore, the mineralization depth of the ore deposit was a medium level.

### 4.5. Inclusion composition

In the ore-forming fluid (Table 2), the main cations are $Na^+$ and $Ca^{2+}$, while the contents of $K^+$ and $Mg^{2+}$ are very low. The variation range of X ($Na^+$)/X ($K^+$) was 2.80–23.76. Except 12SST09-1, in which $NO_3^-$ and $SO_4^{2-}$ have highest concentrations ($39.6 \times 10^{-6}$ and $16.22 \times 10^{-6}$, respectively), all the samples have $SO_4^{2-}$ and $Cl^-$ with the highest concentrations. The content of $NO_3^-$ was the lowest. Thus, the ore-forming fluid primarily belong to the $Na^+$–$Ca^{2+}$–$SO_4^{2-}$ $Cl^-$ system, and only a few samples belong to the $Na^+$–$Ca^{2+}$–$NO_3^-$ $SO_4^{2-}$ system. For the gas phase composition (Table 3), different compositions showed a relationship as follows: $H_2O > CO_2 > H_2 > N_2 > CO > CH_4$. Fig. 6 shows the variation in the gas phase composition of ore-forming fluid. Except that $CO_2$ has a linear relationship with gas-phase $H_2O$ ($R^2 = 0.7442$), $H_2$, $N_2$, CO and $CH_4$ have a poor linear relationship with gas-phase $H_2O$ ($R^2 < 0.3$).

## 5. Geochemical analysis of stable isotopes

### 5.1. Hydrogen and oxygen isotopes

Isotopes in ore-forming fluids of different origins differ significantly (White, 1974). Skarn garnet is the main ore type in the Saishitang ore field. Garnet is one of the rock-forming minerals with the highest stability and the lowest oxygen diffusion rate. Its oxygen isotopic composition can be hardly changed by hydrothermal alteration (Wu et al., 2005). Therefore, garnet can be used as an indicator of the oxygen isotopic composition of crystallizing medium (Wang et al., 2008). The specific sampling locations are shown in Fig. 2b and the hydrogen and oxygen isotopic compositions of fluid inclusions from the Saishitang ore field at the different stages of ore-forming process are shown in Table 4. The hydrogen isotope (δD) in liquid contained in the fluid inclusions from different minerals was tested. Meanwhile, the oxygen isotope ($\delta O_{V\text{-}SMOW}$) was tested in quartz, garnet, diopside and tremolite.

The values of $\delta D_{V\text{-}SMOW}$ of samples from the different stages of ore-forming process vary in the range of −125.9 to −89‰, −130.7 to −132.8‰, −139.9 to −161.2‰ and −105.4 to −89.6‰, respectively. Thus, there was a decrease in $\delta D_{V\text{-}SMOW}$ from rock mass to the skarn stage (I) and to the quartz–sulfide stage (II), but the $\delta D_{V\text{-}SMOW}$ increased from the quartz–sulfide stage (II) to the sulfide quartz–calcite vein stage (III). The values $\delta O_{V\text{-}SMOW}$ of samples from the three metallogenic stages are 12.4–16.9‰ (stage I), 9.8–18.1‰ (stage II-1), 8.3–10.2‰ (stage II-2) and 13.8–14.1‰ (stage III), respectively. The equation for oxygen isotope equilibrium fractionation between minerals and water (Clayton et al., 1972; Lu and Yang, 1982; Zheng et al., 2000) was used for the correction of homogenization temperature of ore-forming fluid. According to the calculations (Table 4), the values of $\delta O_{H2O}$ are 5.240–10.401‰ (stage I), 10.956–15.241‰ (stage II-1), 7.650–11.127‰ (stage II-2) and 2.562–2.862‰ (stage III). The variation range of the first three stages was consistent, while the value of stage III declined.

### 5.2. Sulfur isotopes

The specific sampling locations were shown in Fig. 2b and the sulfur isotopes of sulfides from five samples in the Saishitang ore field were analyzed and are listed in Table 5. Sulfur isotopes for the main mineralization stage of the Saishitang copper deposit have also been studied by Lai et al. (2010) and Li et al. (1993). The sulfur isotopes in our five sulfide samples and those in the previous studies (Lai et al., 2010; Li et al., 1993)

**Table 2**
Liquid phase composition ($\times 10^{-6}$) of fluid inclusions from the Saishitang copper deposit.

| Sample no. | $F^-$ | $Cl^-$ | $NO_3^-$ | $SO_4^{2-}$ | $Na^+$ | $K^+$ | $Mg^{2+}$ | $Ca^{2+}$ | ΣM$^-$ | ΣM$^+$ | $Na^+/K^+$ | $F^-/Cl^-$ | $X(Cl^-)/X(SO_4^{2-})$ | $X(Na^+)/X(Ca^{2+}+Mg^{2+})$ |
|---|---|---|---|---|---|---|---|---|---|---|---|---|---|---|
| 12SST09-1 | 1.46 | 3.515 | 39.6 | 16.22 | 8.779 | 2.64 | 0.4071 | 9.351 | 60.795 | 21.1771 | 3.33 | 0.42 | 0.217 | 0.899 |
| 12SST27 | 0.6943 | 14.77 | 0.0753 | 69.58 | 14.06 | 3.324 | 2.881 | 11.48 | 85.1196 | 31.745 | 4.23 | 0.05 | 0.212 | 0.979 |
| 12SST15 | 0.2611 | 7.893 | 2.889 | 67.98 | 18.24 | 6.521 | 5.092 | 21.15 | 79.0231 | 51.003 | 2.80 | 0.03 | 0.116 | 0.695 |
| 12SST09-2 | 1.049 | 5.15 | 0.1171 | 7.342 | 6.576 | 0.536 | 0.0871 | 0.9428 | 13.6581 | 8.1419 | 12.27 | 0.20 | 0.701 | 6.385 |
| 12SST17 | 0.5363 | 10.28 | 0.133 | 62.73 | 13.63 | 2.154 | 6.866 | 34.98 | 73.6793 | 57.63 | 6.33 | 0.05 | 0.164 | 0.326 |
| 12SST25 | 1.109 | 5.017 | 4.044 | 20.15 | 9.575 | 0.403 | 1.153 | 1.973 | 30.32 | 13.104 | 23.76 | 0.22 | 0.249 | 3.06 |
| 12SST20 | 3.021 | 13.82 | 0.0475 | 29.44 | 16.87 | 0.7514 | 0.092 | 1.595 | 46.3285 | 19.3084 | 22.45 | 0.21 | 0.469 | 10 |

- Not measured data.

**Table 3**
Gaseous phase composition ($\times 10^{-6}$) of fluid inclusions from the Saishitang copper deposit.

| Sample no. | Mineral | $H_2$ | $N_2$ | CO | $CH_4$ | $CO_2$ | $H_2O$ (gas) |
|---|---|---|---|---|---|---|---|
| 12SST09-1 | Quartz | 0.0868 | 0.3921 | 0.5577 | 0.0451 | 2.695 | $4.168 \times 10^5$ |
| 12SST27 | Quartz | 0.3876 | 1.836 | 0.0907 | 0.0781 | 0.7431 | $2.964 \times 10^5$ |
| 12SST15 | Quartz | 0.2378 | 0.2577 | 0.185 | 0.1752 | 3.315 | $1.575 \times 10^5$ |
| 12SST09-2 | Quartz | 0.2304 | 0.1164 | 0.1209 | 0.2255 | 0.3062 | $3.120 \times 10^5$ |
| 12SST17 | Garnet | 2.488 | 0.1266 | 0.1863 | 0.2656 | 2.651 | $2.296 \times 10^5$ |
| 12SST26 | Garnet | 0.1101 | 0.2923 | 0.127 | 0.0105 | 0.6647 | $0.9678 \times 10^5$ |
| 12SST25 | Quartz | 0.0443 | 0.1895 | 0.1009 | 0.3675 | 1.236 | $1.053 \times 10^5$ |
| 12SST24 | Quartz | 0.0821 | 0.2193 | 0.0785 | 0.1873 | 0.5603 | $2.239 \times 10^5$ |
| 12SST20 | Quartz | 0.4525 | 0.6523 | 0.2028 | 0.2386 | 0.8349 | $1.071 \times 10^6$ |

show that the $\delta^{34}S$ values of 24 samples of pyrrhotite are −2.1 to −4.66‰, with an average of 0.03‰ and a standard deviation of 1.65‰; the $\delta^{34}S$ values of 28 pyrite samples are −6.45–4.11‰, with an average of −0.546‰ and a standard deviation of 2.23‰; the $\delta^{34}S$ values of eight chalcopyrite samples are −2.58–2.16‰, with an average of −0.148‰ and a standard deviation of 1.69‰; the $\delta^{34}S$ values of four sphalerite samples are −7.47–0.54‰, with an average of −3.063‰ and a standard deviation of 3.41‰; the $\delta^{34}S$ values of five galena samples are −4.85–5.57‰, with an average of −2.138‰ and a standard deviation of 4.46‰; and the $\delta^{34}S$ value of one arsenopyrite sample was 0.59‰.

Determination of the source of sulfur in ore-forming fluid should be based on the total sulfur isotopic composition of sulfide ($\delta^{34}S_{\Sigma S}$) in hydrothermal fluid in the sedimentary stage. The mineral assemblages containing sulfur but not sulfate in the Saishitang ore field were pyrrhotite, pyrite, chalcopyrite, sphalerite and galena. The dissolved sulfur was mainly in the form of $H_2S$. Thus, the average $\delta^{34}S$ value of sulfides, especially pyrite, can roughly reflect the total sulfur isotopic composition $\delta^{34}S_{\Sigma S}$ of the hydrothermal fluid (Ohmoto, 1972; Liu et al., 2007).

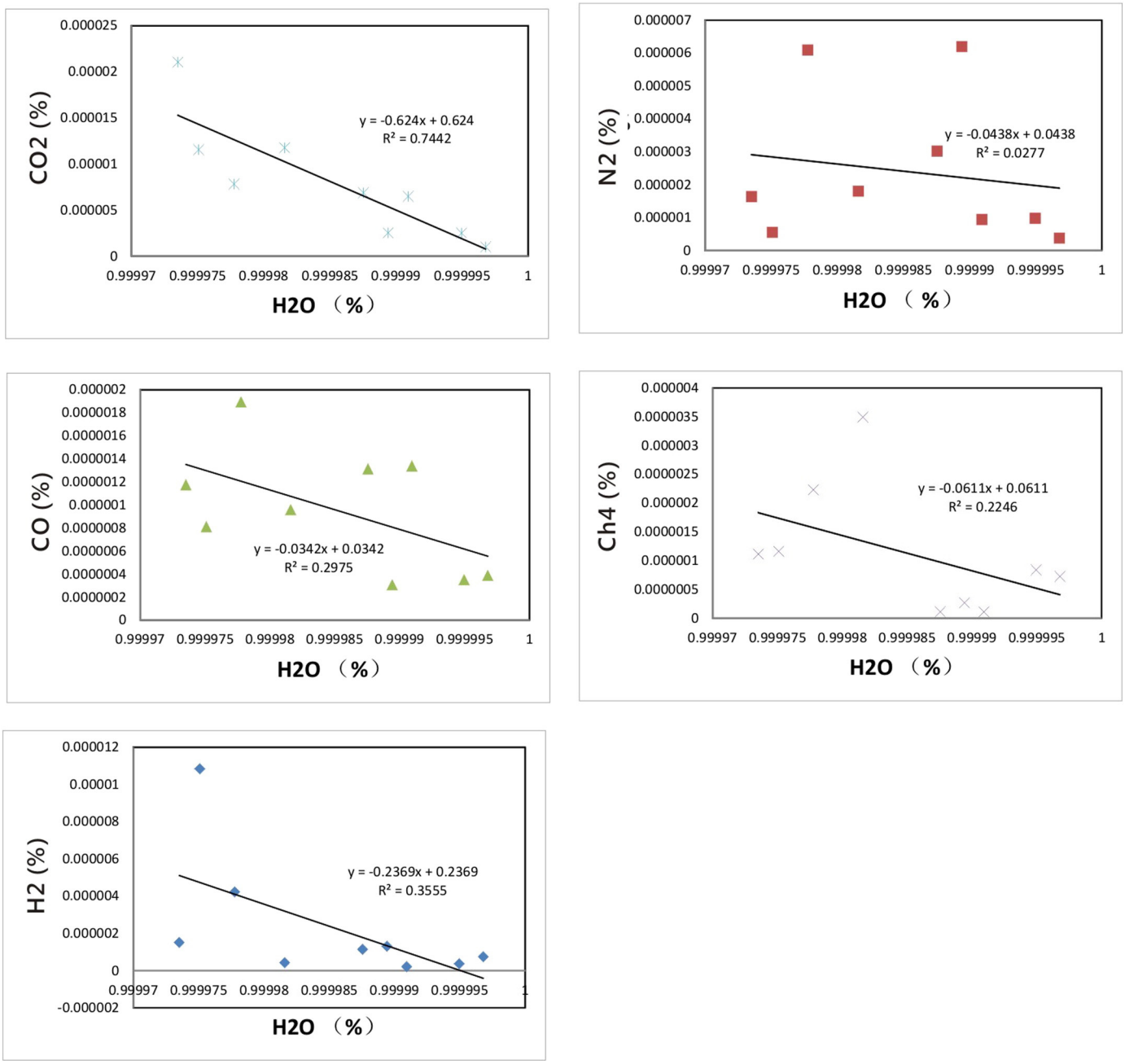


**Fig. 6.** Covariation diagrams of gas composition $CO_2$, $N_2$, CO, $CH_4$, $H_2$ and $H_2O$ in the Saishitang copper deposit.

**Table 4**
Hydrogen and oxygen (‰) of the fluid inclusions in Saishitang copper deposit.

| Stage | | Sample no. | Mineral | $\delta D_{V\text{-}SMOW}$ | $\delta O_{V\text{-}SMOW}$ | $t_h$/°C | $\delta O_{H2O}$ |
|---|---|---|---|---|---|---|---|
| | Quartz diorite | 12SST09-1 | Quartz | −102.4 | 15.7 | 278.16 | 7.979 |
| | | 12SST20 | Quartz | −107.1 | 16.3 | 329.74 | 10.401 |
| | | 12SST15 | Quartz | −89 | 16.9 | 224.87 | 6.672 |
| | | 12SST27 | Quartz | −109.6 | 12.4 | 406.22 | 8.477 |
| | | 12SST09-2 | Quartz | −118.2 | 16.4 | 208.67 | 5.240 |
| | | 12SST16 | Quartz | −125.9 | 16.6 | 224.87 | 6.372 |
| I | Skarn | 12SST26 | Garnet | −130.4 | 11.7 | 396.2 | 12.856 |
| | | 12SST17 | Garnet | −132.8 | 10.2 | 368 | 11.127 |
| | | 12SST28 | Quartz | −130.7 | 18.1 | 461.72 | 15.241 |
| | | 12SST23 | Garnet | −113.2 | 9.8 | 396.2 | 10.956 |
| | | 12SST21 | Diopside | −161.2 | 9.3 | 263.16 | 9.350 |
| II | Quartz sulfide | 12SST18 | Tremolite | −152.7 | 8.3 | 236.47 | 7.708 |
| | | 12SST17 | Diopside | −139.9 | 10.2 | 368 | 11.127 |
| III | Polymetallic sulfide-bearing quartz–calcite vein | 12SST24 | Quartz | −89.6 | 13.8 | 207.38 | 2.562 |
| | | 12SST25 | Quartz | −105.4 | 14.1 | 207.38 | 2.862 |

Note: $\delta^{18}O_{H2O}$ are calculated values, Quartz–Water: $1000\ln = \delta^{18}O_{Mineral}$–$\delta^{18}O_{H2O} = 3.38 \times 10^6\ T^{-2}$–3.4 (Clayton et al., 1972); Garnet-Water: $1000\ln = 1.14 \times 10^6\ T^{-2}$–3.70 (Lu and Yang, 1982); Tremolite–Water: $1000\ln = 3.92 \times 10^6\ T^{-2}$–$8.28 \times 10^3\ T^{-1} + 2.38$ (Zheng et al., 2000); Diopside–Water: $1000\ln = 3.92 \times 10^6\ T^{-2}$–$8.43 \times 10^3\ T^{-1} + 2.04$ (Zheng et al., 2000); $t_h$/°C: complete homogenization temperature.

## 6. Discussion

### 6.1. Origin and evolution of ore-forming fluid

Fluid inclusions and ore-forming fluid have long been the important aspects of research on mineral deposits (e.g., Deng et al., 2001, 2003, 2011; Liu et al., 2011; Cao et al., 2012; Li et al., 2012; Wang et al., 2014; Liu et al., 2000, 2007, 2015a). In the Saishitang ore field, a large number of melt inclusions are detected in porphyritic quartz of magmatic stage and the garnet of skarn stage which are evidence of existence of magmatic fluid (e.g., Lu et al., 2004). The coexistence of melt inclusions and fluid inclusions in this ore field is the indication of magmatic immiscibility. It can be inferred that, in the early mineralization stage, magmatic fluid has a close relationship with the genesis of ore-forming fluid with medium to high temperature and high salinity.

Roedder (1971) found that molar ratios of liquid-phase components of fluid inclusions as $X(Na^+)/X(K^+) < 2$ and $X(Na^+)/X(Ca^{2+} + Mg^{2+}) > 4$ indicate either magma or metamorphic hydrothermal fluid, whereas molar ratios of $X(Na^+)/X(K^+) > 2$ and $(Na^+)/(Ca^{2+} + Mg^{2+}) < 1.5$ indicate hot brine or formation water. For the rock mass in the Saishitang ore field, the ranges of measured $X(Na^+) / X(K^+)$ ratios and $X (Na^+)/X(Ca^{2+} + Mg^{2+})$ ratios are 2.80–12.27 and 0.695–6.385, respectively, indicating mixture of magmatic and formation water. However, for inclusions at dry-wet skarn (stages I and II), the ranges of measured $X (Na^+)/X(K^+)$ ratio and $X(Na^+)/X(Ca^{2+} + Mg^{2+})$ ratio are 1.30–6.33 and 0.404–0.979, respectively, indicating formation water. For stage III and the late hydrothermal alteration stage, the measured $X (Na^+)/X(K^+)$ ratios are 23.76 and 22.45 and the measured $X (Na^+)/X(Ca^{2+} + Mg^{2+})$ ratios are 3.06 and 10, indicating mixture of magmatic and formation water. A small $X (F^-)/(Cl^-)$ ratio usually indicates genesis related to underground hot brine or atmospheric precipitation (Lu et al., 1990). In the Saishitang ore field, the measured $X (F^-)/(Cl^-)$ ratios are 0.05–0.42, indicating genesis related to formation water. The $SO_4^{2-}$ in solution represents all sulfur-bearing phases in fluid inclusions, such as $S^{2-}$, $HS^-$ and $SO_4^{2-}$(Chen et al., 2004). The intrusion of diorite porphyry may introduce a large concentration of $SO_2$ (Fan et al., 2010). Moreover, the high $SO_4^{2-}$ concentration in the ore-forming fluid is also evidence of the existence of magmatic hydrothermal fluid (Jiang et al., 1994). In the Saishitang ore field, the content of $SO_4^{2-}$ was high at all stages (7.342–76.369), indicating genesis related to magmatic water. Thus, magmatic and formation water coexist in this ore field.

**Table 5**
Sulfur isotopic composition of ore sulfides from the Saishitang copper deposit.

| Sample no. | Determination of mineral | $\delta^{34}$SV-CDT(‰) |
|---|---|---|
| 12SST05 | Pyrite | −1.2 |
| 12SST11 | Pyrite | −3.2 |
| 12SST12 | Pyrite | −3.2 |
| 12SST24 | Chalcopyrite | 0.4 |
| 12SST25 | Chalcopyrite | 1.2 |

The variation of gas-phase components of ore-forming fluid (Fig. 6) shows that only $CO_2$ had a good linear relationship with gas-phase $H_2O$ ($R^2 = 0.7442$) whereas $H_2$, $N_2$, CO and $CH_4$ had a poor linear relationship with gas-phase $H_2O$ ($R^2 < 0.3$). If the good linear relationship between $CO_2$ and $H_2O$ was caused by phase separation, then the same process would govern the relationship between other gases and $H_2O$. During phase separation, these gases are fractionated into gas phase along with $CO_2$, which can result in consistent variations of each gas-phase component and $H_2O$. This means a high degree of linear fitting (Li and Liu, 2002; Liu et al., 2003; Li et al., 2013). In addition, if the mixed magmatic and formation fluids both contained $CO_2$, it could be a reason of good linear relationship between $CO_2$ and gas-phase $H_2O$. However, Fig. 6 shows that each gas-phase component in ore-forming fluid was not formed by separation of the same phase. Instead, external fluid was mixed with the ore-forming fluid during migration, leading to the introduction of gas-phase components at different proportions.

In general, the earth surface system (especially the atmosphere) is enriched with $N_2$ and Ar compared with the earth interior. Therefore, surface atmospheric precipitation and basinal hot brine have higher $N_2$ and Ar content compared with deep magma or metamorphic water (Chen et al., 2001; Zhang et al., 2007). Deep magmatic water has low content of $N_2$ and Ar, with $X(N_2)/X(Ar)$ ratio generally larger than 200 (Norman and Musgranve, 1994; Norman et al., 1996). In the Saishitang ore field, a very low $N_2$ content was detected ($0.1164–0.3921 \times 10^{-6}$), and no argon gas was found, indicating deep source of magmatic water.

As seen from the $\delta D$–$\delta^{18}O_{H2O}$ plot (Fig. 7), the obtained data for each stage of ore-forming process all fall within the range of existence of formation water below the primary magmatic water. The rock mass samples resemble the primary magmatic water on the $\delta D$–$\delta^{18}O_{H2O}$ plot. Most of them belong to the initial mixed magmatic water proposed by Zhang (1985). It is indicated that the ore-forming fluid at this stage may have been already mixed with hydrothermal fluid with low $\delta D$ values, resulting in the reduction of $\delta D$ values. However, the $\delta D$ values of stages I and II gradually decreased while the $\delta^{18}O_{H2O}$ values increased slightly. This suggests that the mixed hydrothermal fluid has low $\delta D$ values and high $\delta^{18}O_{H2O}$ values. The samples at stage III fall on the left of the initial mixed magmatic water, indicating a shift towards the meteoric water line.

In addition, samples of quartz diorite and stages I and II-1 all have fluid inclusions with high homogeneous temperatures and high

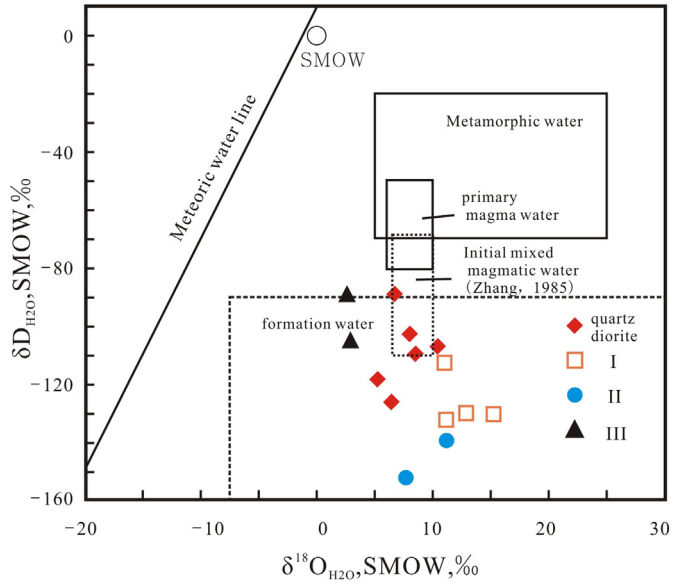


**Fig. 7.** δD versus $\delta^{18}O_{H2O}$ for ore forming fluids from the Saishitang copper deposit. (The base diagram is cited from Sheppard (1986). The meteoric water line is cited from Epstein et al. (1965). Data are from Table 4).

salinities indicating the existence of magmatic fluid. Therefore, the Saishitang ore field has both magmatic fluid and formation water (probably as hot brine). Along with the process of fluid evolution, the temperature of ore-forming fluid gradually decreased, with an increased proportion of formation water mixed into the ore-forming fluid. As a result, the types of fluid inclusions of the main metallogenic stage (stage II-1) changed significantly, from type G + W inclusions representing magmatic hydrothermal fluid to the coexistence of types H and W inclusions. In the late quartz–calcite vein stage, features of magmatic water mixed with atmospheric precipitation were also detected, indicating that the ore field has undergone a complex process of fluid mixing and evolution.

### 6.2. Source of metallogenic materials

The results of previous Pb isotope studies (Zhu et al., 2012; Li et al., 2009) of ores from the main mineralization stage of the Saishitang ore field indicated a strong homogeneity of Pb isotopes: $^{208}Pb/^{204}Pb$ = 37.943–38.672, with average of 38.249; $^{207}Pb/^{204}Pb$ = 15.442–15.721, with average of 15.563; $^{206}Pb/^{204}Pb$ = 17.901–19.108, with average of 18.373. Their μ values also had strong homogeneity (9.18–9.7), with average of 9.396. These features indicate that the Pb isotopic composition of fluids in the Saishitang ore field is strongly homogeneous.

The coexistence of magmatic fluid and formation water is proved in the main metallogenic stage of the ore field. However, stable isotope evidence is still needed to determine the source of metallogenic materials. The $\delta^{34}S$ values of sulfides in the ore field are concentrated in the interval of −6.45 to −5.57‰, with average of −0.546‰. As seen from the histogram of sulfur isotopic composition (Fig. 8), the $\delta^{34}S$ values are mainly distributed near zero with a peak occurring around −2.0 to −1.0‰. This $\delta^{34}S$ data distribution pattern reflects the characteristics of magmatic sulfur (Ohmoto and Rye, 1979).

The Pb isotope diagram (Fig. 9) and Δγ–Δβ diagram (Fig. 10a) show that the metallogenic materials mainly originate from magmatic hydrothermal fluid related to crust–mantle mixing in an orogenic environment. On the $^{207}Pb/^{204}Pb$–$^{206}Pb/^{204}Pb$ diagram (Fig. 10b) for judging the tectonic setting of source region, most of the data fall on the lower crust, MORB and PREMA. It is inferred that the crust–mantle interaction related to metallogenic process occurred at the interface between the upper mantle and the lower crust.

The sulfur and lead isotope data suggest that the metallogenic materials have a close connection with magmatic fluid.

### 6.3. Metallogenic mechanism

The plot of homogenization temperature versus salinity of fluid inclusions can be used to determine the evolutionary trend of fluid (e.g., Zhai et al., 2012). The present study shows that there exists a positive correlation between homogenization temperature and salinity of fluid inclusions trapped in fluid mixing and between salinity and enthalpy. However, the correlation is negative for fluid inclusions trapped in the process of fluid boiling or phase separation (Shepherd et al., 1985). As shown by the fluid evolution diagram (Fig. 11), magmatic fluid is high-temperature and high-salinity fluid. Such fluid is mixed with low-temperature and low-salinity fluid at skarn stage (I). Three types of fluid inclusions coexist in the same host mineral at stage II-1 (sample 12SST-12) with various modes of homogenization, similar homogenization temperatures

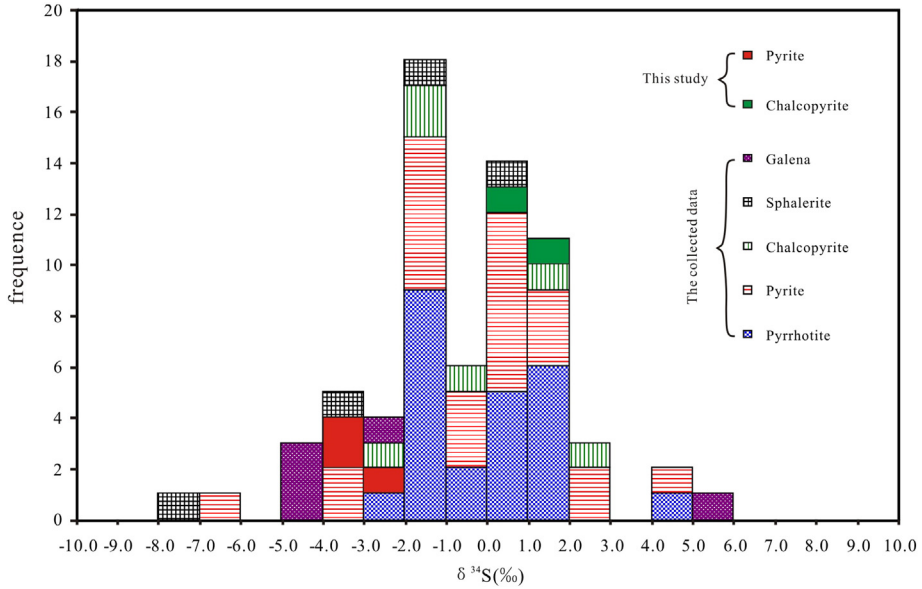


**Fig. 8.** Frequency histogram of $\delta^{34}S$ for ore sulfides from the Saishitang copper deposit.

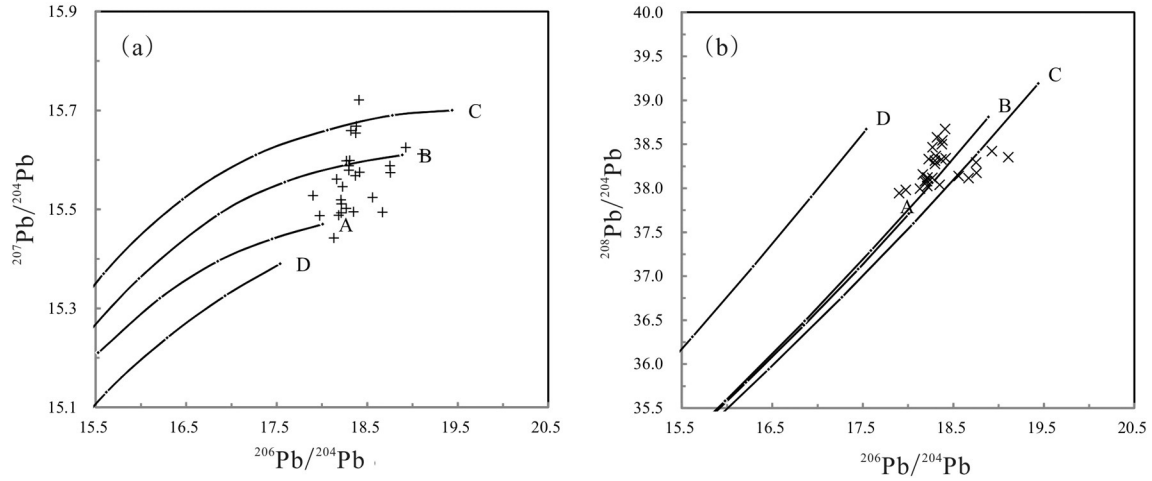


**Fig. 9.** The plumbotectonic model for the Saishitang copper deposit (the base map after Zartman and Doe, 1981; data from Zhu et al., 2012; Li et al., 2009) (A — Mantle; B — Orogen; C — Upper Crust; D — Lower Crust).

and great differences in salinity. Due to the existence of boiling inclusion assemblage (Fig. 4i, j), the trapped fluid is a saturated or supersaturated fluid that was boiling (Chen et al., 2010). With a reduction in pressure at this stage, decompression boiling took place.

The migration of metal ions such as Cu and Mo mainly occurs in the form of complex. Under condition of high temperature and high pressure, especially the critical or supercritical state, complexes have high stability. As decompression boiling proceeds at stage II-1, several volatile components such as $CO_2$, $H_2O$, $CH_4$ and $N_2$ escaped, resulting in the increase of pH and fluid salinity. As temperature decreased, the physical and chemical equilibrium of the original system was disrupted, resulting in the deposition of metal sulfides (e.g., chalcopyrite, pyrite and bornite) (Rui et al., 1984). Extensive studies (e.g., Zhang, 1997; Reed and Palandri, 2006; Wu et al., 2010; Gu et al., 2010; Wang et al., 2011) have shown that boiling of hydrothermal fluid can significantly alter the phase equilibrium of hydrothermal fluid. Phase changes facilitate decomposition of metal complexes in hydrothermal fluid, causing precipitation of a large amount of metal sulfides and thus forming metallic minerals. Decompression boiling of fluid occurred at the main metallogenic stage (II-1), leading to changes of physical and chemical conditions of pH, $E_h$, $f_{O2}$ and $f_{S2}$. Thus, metallic elements such as Cu in the fluid no longer existed in the stable form of complex, and precipitated from the hydrothermal fluid.

The H–O isotope plot (Table 4, Fig. 7) shows that a larger amount of formation water was involved at the skarn stage (II-2) because there was a significant reduction of temperature and salinity of inclusions (Fig. 11b). Moreover, the minerals formed at this stage are located far away from the rock mass. There is the possibility that the mixing and interaction of magmatic water and formation water helped to preserve the products of the stratification of surrounding rock.

The Saishitang ore field is located at the transition zone between two E–W-trending orogenic belts, i.e., the WQOB and the Eastern Kunlun orogenic belt. The joining and transition of the two orogenic belts correspond to the formation of the Gonghe aulacogen and its evolution with composite superimposition. It had basically experienced the plate tectonic system of the Triassic or even earlier and the intracontinental orogenic system since the Jurassic. The WQOB was already connected with Eastern Kunlun orogenic belt at the end of Middle Triassic. Then, the two connected orogenic belts experienced intracontinental orogeny and composite superimposed reformation as a whole (Sun, 2004).

A recent investigation (Yan et al., 2012) has found that the formation of the Saishitang copper deposit, Tongyugou copper deposits, Gakehe copper–silver–arsenic ore deposits and Lajiehai molybdenum–copper ore deposits are closely related to the magmatic activity of granitic rocks, including Triassic quartz diorite, diorite porphyrite, plagiogranite porphyry and quartz porphyry. Geochemical analyses in Liu et al. (2012) show that these granitic rocks belong to calc-alkaline/high-K calc-alkaline/shoshonite assemblage. The granitic rocks possess geochemical features of extensional setting and crust–mantle mixing (She et al., 2007; Wang et al., 2009; Li et al., 2009). Local tectonic extension could have helped the change of ore-forming pressure from lithostatic pressure to hydrostatic pressure. An abrupt decline of pressure could have caused the boiling of ore-forming fluid and promoted the deposition and enrichment of minerals along with the decline of temperature (e.g., Meinert et al., 2003). The $\delta^{34}S$ values (−6.45–5.57‰) and Pb isotope analysis of the Saishitang ore field indicate that the metallogenic materials were mainly derived from the deep crust and have a certain affinity with the granite of Eastern Kunlun Mountains(Li et al., 2009). Moreover, the zircon U–Pb age of quartz diorite was 221.7–223.5 Ma (unpublished), suggesting close relationship with the Middle to Late Triassic magmatic activity of Western Qinling Mountains and Saishitang–Tongyugou belt.

## 7. Conclusions

(1) Hydrothermal activity in the Saishitang skarn-type copper ore field can be divided into three stages: skarn stage (I), quartz–sulfide stage (II) and sulfide-bearing quartz–calcite vein stage (III). The quartz–sulfide stage can be subdivided into a massive sulfide stage (II-1) and a layered sulfide stage (II-2).

(2) From the magmatic (quartz diorite) stage to each metallogenic stage (I, II-1, II-2, III), the ore-forming fluid showed a decreasing trend of homogenization temperature, salinity and density.

(3) The ore-forming fluid mainly belong to a $Na^+$–$Ca^{2+}$–$SO_4^{2-}$ $Cl^-$ system, and partly belong to a $Na^+$–$Ca^{2+}$–$NO_3^-$ $SO_4^{2-}$ system, and was formed by mixing of magmatic and formation water. As the fluid evolution proceeds, more formation water was mixed with the ore-forming fluid, and there existed the mixing of atmospheric precipitation at sulfide-bearing quartz vein stage. The mixing of magmatic hydrothermal fluid and formation water led to the formation of skarn.

(4) Petrographic and stable isotope analyses of fluid inclusions indicate that the metallogenic materials have a close connection with magmatic fluid.

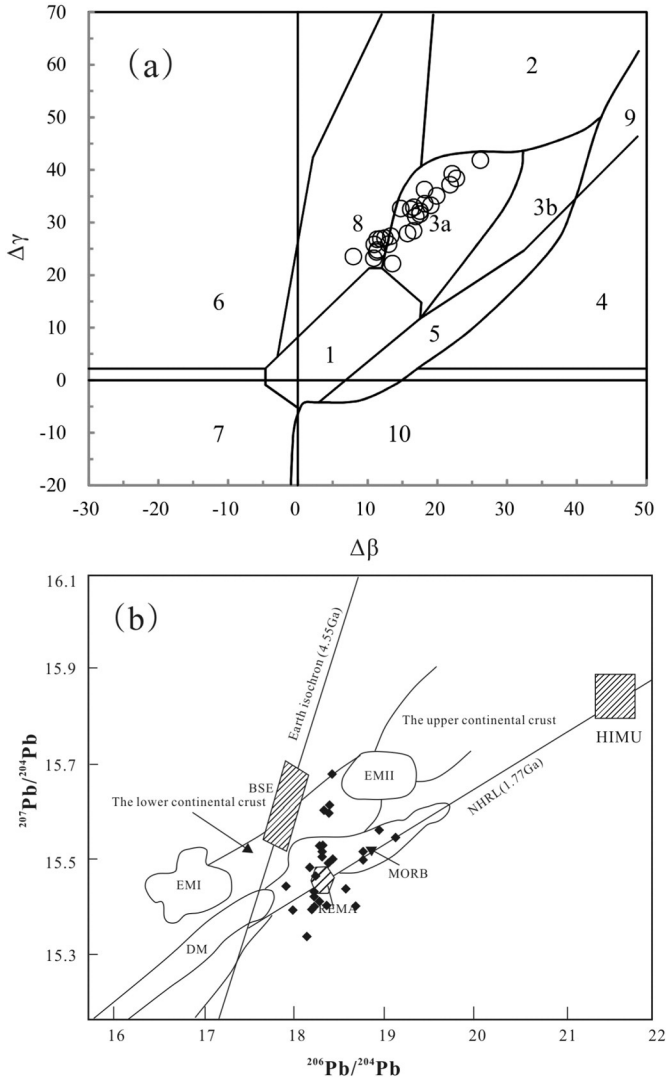


**Fig. 10.** a-Δγ–Δβ diagram of the Pb isotopic (after Zhu et al., 2001), b-The $^{207}Pb/^{204}Pb$-$^{206}Pb/^{204}Pb$ diagrams of the lamprophyres from Saishitang (after Norman and Musgrave, 1994) (date from Rollison, 1993; Li et al., 2009) 1 — The mantle source lead; 2 — Upper crust lead; 3 — The subduction zone lead of mixing of upper crust and mantle (3a — Magmatism; 3b — Sedimentary); 4 — Chemical deposition lead; 5 — Hydrothermal effects lead; 6 — Medial-deep metamorphism lead; 7 — deep metamorphism of lower crust lead; 8 — Orogen lead; 9 — Ancient shale upper crust lead; 10 — Retrograde lead.

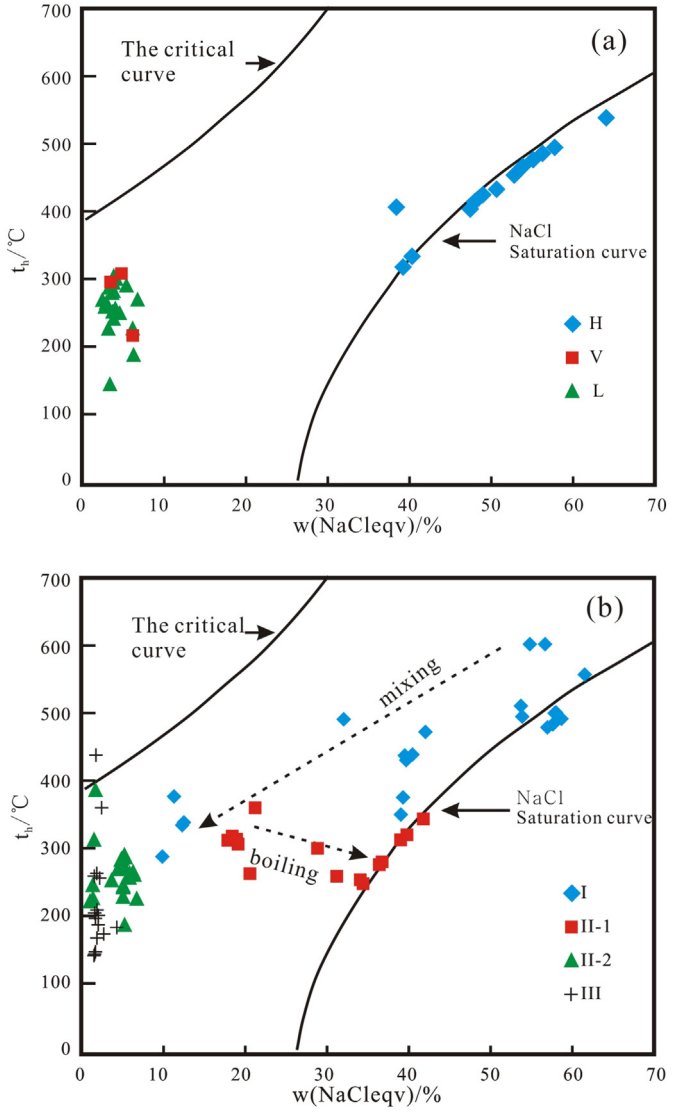


**Fig. 11.** w($NaCl_{eqv}$) phase diagram of fluid inclusions in the Saishitang porphyry copper deposit(a-quartz diorite; b- I, II, III stage).

## Acknowledgments

We are particularly grateful to Prof. Hao Ziguo, Dr. Lu Yanming, and Dr. Qingmin, as well as the guest editor of this special issue for their helpful and constructive comments. This manuscript has benefitted significantly from constructive suggestions of Dr. Guo Xiaodong and Dr. Li Gongjian. We appreciate Zhu Huiyan and Liu Mu for their kind assistance with the temperature measurement of fluid inclusions and isotopic analyses. We also thank Liu Heng, Liu Henan and all the employees of Hydrological station of Tangnaihai Township for their generous help during the fieldwork. This study was jointly funded by the Geological Survey Project of China (Grant 1212011220924), the Geological Survey Projects of China Geological Survey (Grant 1212011220899), and the National Natural Science Foundation of China (Grant 41030423).

## References

An, J.H., 2010. The Characteristics of Fluid Inclusions and Mineralization of the SaiShitang Cu–Polymetallic Deposit, Qinghai Province. Central South University, Changsha, pp. 1–32 (in Chinese with English abstract).

Bodnar, R.J., Vityk, M.O., 1994. In: De Vivo, B., Frezzotti, M.L. (Eds.), Interpretation of Microthermometric Data for $H_2O$–NaCl Fluid Inclusions. In Fluid Inclusions in Minerals, Methods and Applications. Virginia Tech, Blacksburg, VA, pp. 117–130.

Cao, Y., Carranza, E.J.M., Li, S.Y., Yao, M.J., Zhang, H.F., 2012. Source and evolution of fluids in the Shihu gold deposit, Taihang Mountains, China: evidence from microthermometry, chemical composition and noble gas isotope of fluid inclusions. Geochem. Explor. Environ. Anal. 12, 177–191.

Chen, W.J., Liu, J.M., Liu, H., Sun, X.G., Zhang, R.B., Zhang, Z.L., Qin, F., 2010. Geochronology and fluid inclusion study of the Jiguanshan porphyry Mo deposit, Inner Mongolia. Acta Petrol. Sin. 26 (5), 1423–1436 (in Chinese with English abstract).

Chen, Y.J., Li, J., Pirajno, F., Lin, Z.J., Wang, H.H., 2004. Hydrothermal metallogeny of the Shanggong gold deposit, East Qinling: studies on ore geology and fluid inclusion geochemistry. J. Mineral. Petrol. 24 (3), 1–2 (in Chinese with English abstract).

Chen, Y.J., Sui, Y.H., Gao, X.L., 2001. Fluid geochemistry of Tieluping Ag ore and its implications for the CPMF model. Water–Rock Interaction. Lisse: Swets and Zeitlinger, pp. 689–692.

Clayton, R.N., O'Neil, J.R., Mayeda, T.K., 1972. Oxygen isotope exchange between quartz and water. J. Geophys. Res. 77 (7), 3057–3067.

Deng, J., Fang, Y., Yang, L.Q., Yang, J.C., Sun, Z.S., Wang, J.P., Ding, S.J., Wang, Q.F., 2001. Numerical modeling of ore-forming dynamics of fractal dispersive fluid systems. Acta Geol. Sin. 75 (2), 220–232.

Deng, J., Liu, W., Sun, Z.S., Wang, J.P., Wang, Q.F., Zhang, Q.X., Wei, Y.G., 2003. Evidence of mantle-rooted fluids and multi-level circulation ore-forming dynamics: a case study from the Xiadian gold deposit, Shandong Province, China. Sci. China Series D 46 (Suppl), 123–134.
Deng, J., Wang, Q.F., Xiao, C.H., Yang, L.Q., Liu, H., Gong, Q.J., Zhang, J., 2011. Tectonic–magmatic–metallogenic system, Tongling ore cluster region, Anhui Province, China. Int. Geol. Rev. 53 (5–6), 449–476.
Epstein, S., Sharp, R.P., Gow, A.J., 1965. Six-year record of oxygen and hydrogen isotope variations in South Pole firn. J. Geophys. Res. 70 (8), 1809–1814.
Hall, D.L., Sterner, S.M., Bodnar, R.J., 1988. Freezing point depression of NaCl–KCl–$H_2O$ solutions. Econ. Geol. 83 (1), 197–202.
Gu, X.X., Liu, L., Dong, S.Y., Zhang, Y.M., Li, K., Li, B.H., 2010. Immiscibility during mineralization of Yinan Au–Cu–Fe deposit, Shandong Province: evidence from fluid inclusions and H–O isotopes. Mineral Deposits 29 (1), 43–57 (in Chinese with English abstrct).
Fan, H.R., Y.H., Xie, Zhai, M.G., Jin, C.W., 2003. A three stage fluid flow model for Xiaoqinling lode gold metallogenesis in the He'nan and Shanxi Provinces, central China. Acta Petrol. Sin. 19 (2), 260–266 (in Chinese with English abstrct).
Fan, Y., Zhou, T.F., Yuan, F., Tang, M.H., Zhang, L.J., Ma, L., Xie, J., 2010. High sulfidation epithermal hydrothermal system in Lu-Zong volcanic basin: evidence from geological characteristics and sulfur isotope data of Fanshan alunite deposit. Acta Petrol. Sin. 26 (12), 3657–3666 (in Chinese with English abstract).
Hou, L., Ding, J., Wang, C.M., Liao, Z.W., Guo, Y., Wang, S.W., Wang, Z.Z., 2013. Ore-forming fluid and metallogenesis of the Yinachang Fe–Cu–Au–REE deposit, Wuding, Yunan Province, China. Acta Petrol. Sin. 29 (4), 1187–1202 (in Chinese with English abstract).
Jiang, Y.H., Chen, H.N., Wu, Q.H., Chen, S.Z., 1994. Geological characteristics, genesis and further prospecting direction of Ag–Pb–Zn mineralization of Qinxi–Guansi, Zhouning, Fujian. Geophys. Prospect. 30 (4), 21–25 (in Chinese with English abstract).
Lai, J.Q., An, J.H., Wang, X.J., Mao, Y., Song, Z.Y., Cao, Y.H., Tao, J.J., Guo, Z.J., Wang, J., 2010. Geochemical characteristics and tectonic environment analysis of the intrusive rocks in Saishitang ore field. Mineral Resour. Geol. 24 (5), 460–465 (in Chinese with English abstract).
Li, D.S., Kui, M.J., Gu, F.B., Wang, J.J., Bai, H.X., Zhang, F.Y., Wang, F.M., Ma, Y.Q., 2009. Geological characteristics and genesis of the Saishitang copper deposit in Qinghai Province. Acta Geol. Sin. 83 (5), 719–730 (in Chinese with English abstract).
Li, F.D., Zhang, H.W., Song, Z.J., 1993. Thermal Water Metallogenic Model in Ngola Shan Region. Xi'an Jiaotong University Press, pp. 1–144 (in Chinese).
Li, G.J., Wang, Q.F., Zhu, H.P., Yuan, W.M., Gong, Q.J., 2013. Fluids inclusion constraints on the origin of the Shiduolong hydrothermal vein-type Mo–Pb–Zn deposit, Qinghai Province. Acta Petrol. Sin. 29 (4), 1377–1391 (in Chinese with English abstract).
Li, J., Chen, Y.J., Li, Q.Z., Lai, Y., Yang, R.S., Mao, S.D., 2007. Fluid inclusion geochemistry and genetic type of the Yangshan gold deposit, Gansu, China. Acta Petrol. Sin. 23 (9), 2144–2154 (in Chinese with English abstract).
Li, N., Carranza, E.J.M., Ni, Z., Guo, D., 2012. The $CO_2$-rich magmatic–hydrothermal fluid of the Qiyugou breccia pipe, Henan Province, China: implication for breccia genesis and gold mineralization. Geochem. Explor. Environ. Anal. 12, 147–160.
Li, X.J., Liu, W., 2002. Fluid inclusion and stable isotope constraints on the genesis of the Mazhuangshan gold deposit, eastern Tianshan Mountains of China. Acta Petrol. Sin. 18 (4), 551–558 (in Chinese with English abstract).
Lin, D.J., 1983. The geology characters and ore genesis of Saishitang copper deposit in Qinghai. Northwest. Geol. 4, 30–39 (in Chinese with English abstract).
Liu, B., Duan, G.X., 1987. The density and isochoric formulae for NaCl–$H_2O$ fluid inclusions (salinity ≤ 25%) and their applications. Acta Mineral. Sin. 7, 345–352 (in Chinese with English abstract).
Liu, B., Shen, K., 1999. Fluid Inclusion Thermodynamics. Geology Publishing House, Beijing, pp. 1–290 (in Chinese).
Liu, B., 2001. Density and isochoric formulae fore NaCl–$H_2O$ inclusions with medium and high salinity and their applications. Geogr. Rev. 47, 617–622 (in Chinese with English abstract).
Liu, J.J., Zheng, M.H., Liu, J.M., Su, W.C., 2000. Geochemistry of the La'erma and Qiongmo Au–Se deposits in the western Qinling Mountains, China. Ore Geol. Rev. 17, 91–111.
Liu, J.J., Zheng, M.H., Cook, N.J., Long, X.R., Deng, J., Zhai, Y.S., 2007. Geological and geochemical characteristics of the Sawaya'erdun gold deposit, southwestern Chinese Tianshan Mountains. Ore Geol. Rev. 32, 125–156.
Liu, J.J., Dai, H.Z., Zhai, D.G., Wang, J.P., Wang, Y.H., Yang, L.B., Mao, G.J., Liu, X.H., Liao, Y.F., Yu, C., Li, Q.Z., 2015a. Geological and geochemical characteristics and formation mechanisms of the Zhaishang Carlin-like type gold deposit, western Qinling Mountains, China. Ore Geol. Rev. 64, 273–298.
Liu, J.J., Liu, C.H., Carranza, E.J.M., Li, Y.J., Mao, Z.H., Wang, J.P., Wang, Y.H., Zhang, J., Zhai, D.G., Zhang, H.F., Shan, L., Zhu, L.M., Lu, L.K., 2015b. Geological characteristics and ore-forming process of the gold deposits in the western Qinling region, China. Journal of Asian Earth Sci. 103, 332–349.
Liu, J.P., Lai, J.Q., Gu, X.P., Wang, X.J., Mao, Y., Song, W.B., 2012. Geochemistry and zircon LA–ICPMS U–Pb geochronology of intrusive body in Saishitang copper deposit, Qinghai Province, China. Chin. J. Nonferrous Metals 22 (3), 622–632 (in Chinese with English abstract).
Liu, W., Li, X.J., Deng, J., 2003. Sources of ore-forming fluids and metallic materials in the Jinwozi lode gold deposit, eastern Tianshan Mountains of China. Sci. China Series D 46 (Suppl.), 135–153.
Liu, Z.T., Ren, J.Q., Wu, J.R., Huang, Z.H., Lu, H.Q., Wang, H.Y., Zhang, M.F., Peng, X.G., Pang, G.L., 2008a. Qinghai Copper Deposits. Geological Publishing House, Beijing, pp. 1–291 (in Chinese with English abstract).
Liu, Y.C., Hou, Z.Q., Yang, Z.S., Tian, S.H., Yang, T.N., Song, Y.C., Zhang, H.R., Carranza, E.J.M., 2011. Formation of the Dongmozhazhua Pb–Zn deposit in the thrust–fold setting of the Tibetan Plateau, China: evidence from fluid inclusion and stable isotopes. Resour. Geol. 61, 384–406.
Liu, Z.T., Ren, J.Q., Wu, J.R., Huang, C.I., Lu, H.-q., Wang, H.Y., Zhang, M.F., Peng, X.G., Pang, C.L., 2008b. Qinghai Copper Deposits [M]. Geological Publishing House, Beijing, pp. 1–291.
Lu, H.Z., Fan, H.R., Ni, P., Ou, G.X., Shen, K., Zhang, W.H., 2004. Fluid Inclusion. Science Press, Beijing, pp. 249–256 (in Chinese).
Lu, H.Z., 1990a. On fluid–melt inclusions. Geochinica 3, 225–229 (in Chinese with English abstract).
Lu, H.Z., Li, B.L., Shen, K., Zhao, X.H., Yu, T.J., Wei, J.X., 1990. Geochemistry of Fluid Inclusion. Geological Publishing House, Beijing, pp. 153–154 (in Chinese with English abstract).
Lu, W.C., Yang, S.Q., 1982. Use of oxygen bonds to calculate fractionation on equations of oxygen isotope for minerals containing kyanite and staurolite. J. Mineral. Petrol. 2, 106–112 (in Chinese with English abstract).
Lu, Y.F., 1990b. Geochemical characters and ore genesis of Saishitang–Rilonggou mineral zone. Northwest. Geol. 3, 20–26 (in Chinese with English abstract).
Meinert, L.D., Hedenquist., J.W., Satoh, H., 2003. Format ion of anhydrous and hydrous skarn in Cu Au ore deposits by magmatic fluids[J]. Econ. Geogr. 98, 147–156.
Norman, D.I., Musgrave, J., 1994. N2–Ar–He compositions in fluid inclusions: indicators of fluid source. Geochin. Cosmochin. Acta 58 (3), 1119–1131.
Norman, D.I., Moor, J.N., Vonaka, B., 1996. Gaseous species in fluid inclusions: a tracer of fluids and indicator of fluid processes. Proceedings of the 21st Workshop on Geothermal Reservoir Engineering. Stanford: Stanford University, pp. 233–240.
Ohmoto, H., 1972. Systematic of sulfur and carbon isotopes in hydrothermal ore deposits. Economic Geology 7 (5), 551–578.
Ohmoto, H., Rye, R.O., 1979. Isotope of sulfur and carbon. In: Barnes, H.L. (Ed.), Geochemistry of Hydrothermal Ore Deposit, second ed. John Wiley & Sons, New York, pp. 509–567.
Qiu, F.Q., Dong, J.S., 1978. The characters of magma and its mineralization in Saishitang copper deposit in Qinghai Province. Qinghai Geol. 3, 1–19 (in Chinese with English abstract).
Reed, M.H., Palandri, J., 2006. Sulfide mineral precipitation from hydrothermal fluids. Rev. Mineral. Geochem. 61 (1), 609–631. http://dx.doi.org/10.2138/rmg.2006.61.11.
Roedder, E., 1971. Fluid inclusions studies on the porphyry-type ore deposits at Bingham, Utah, Butte, Montana, and Climax, Colorado. Econ. Geol. 66 (1), 98–120.
Roedder, E., 1992. Fluid inclusion evidence for immiscibility in magmatic differentiation. Geochim. Cosmochim. Acta 56, 5–20.
Roedder, E., 1994. Fluid inclusion evidence of mantle fluids. In: De Vivo, B., Frezzotti, M.L. (Eds.), Fluid Inclusion in Minerals, Methods and Applications. Virginia Tech., Blacksburg, pp. 283–296.
Roedder, E., Bodnar, R.J., 1980. Geologic pressure determinations form fluid inclusion studies. Annu. Rev. Earth Planet. Sci. 8, 263–301.
Rollison, H.R., 1993. Using geochemical data: Evaluation, presentation, interpretation. Longman Publishing Group, Longman, p. 352.
Rui, Z., Huang, C.K., Qi, G.M., Xu, J., Zhang, H.T., 1984. Porphyry Copper ( Molybdenum ) Deposits of China. Geol. Pub. House, Beijing, pp. 1–350 (in Chinese).
Shao, J.L., 1990. Gold Exploration Mineralogy. China University of Geoscience Press, Beijing, pp. 1–225 (in Chinese).
Shepherd, T.J., Rankin, A.H., Alderton, D.H.M., 1985. A Practical Guide to Fluid Inclusion Studies. Chapman & Hall, Blackie.
Sheppard, S.M.F., 1986. Characterization and isotopic variations in natural water. Rev. Mineral. 16 (1), 165–183.
She, H.Q., Zhang, D.Q., Jing, X.Y., Tian, S.C., Zhu, H.P., Feng, C.Y., 2007. Characteristics and metallogenesis of Wulanwuzhuer porphyry copper deposit in Qinghai Province. Geol. China 34 (2), 306–314 (in Chinese with English abstract).
Song, Z.J., Zhang, H.W., Li, W.M., Zhang, X.G., Wang, W., 1995. Metallogenic condition and model of coppermultimetal deposits in Ngola Shan region, Qinghai Province. Northwest Geosci. 16 (1), 134–144 (in Chinese with English abstract).
Sun, Y.G., 2004. Gonghe Aulacogen, and Conjugate and Transfer Between the West Qinling and East Kunlun Orogens. Northwest University.
Tian, S.Y., 1999. Relations between magmatic rocks and metallization of the Saishitang–Rilonggou ore field in Qinghai Province. Geol. Explor. Non-Ferrous Met. 8 (6), 383–387 (in Chinese with English abstract).
Touret, J.L.R., Frezzotti, M.L., 1993. Magmatic remnants in plutonic rocks. Bull. Soc. Geol. Fr. 164, 229–242.
Wang, D., Lu, H.Z., Bi, X.W., 2011. Comparison of characteristics of ore forming fluids between quartz–vein tungsten deposits and porphyry copper deposits associated with granitic rocks. Earth Sci. Front. 18 (5), 121–131 (in Chinese with English abstract).
Wang, J.P., Liu, J.J., Carranza, E.J.M., Liu, Z.J., Liu, B., Wang, K.X., Zeng, X.T., Wang, H., Liu, C.H., 2014. A possible genetic model of the Shuangwang hydrothermal breccia gold deposit, Shaanxi Province, central China: evidence from fluid inclusion and stable isotope. J. Asian Earth Sci. 111, 840–852.
Wang, S., Feng, C.Y., Li, S.J., Jiang, J.H., Li, D.S., Su, S.S., 2009. Zircon SHRIMP U–Pb dating of granodiorite Kaerqueka polymetallic ore deposit, Qimantage Mountain, Qinghai Province, and its geological implications. Geol. China 36 (1), 74–84 (in Chinese with English abstract).
Wang, S.X., Zhang, X.C., Leng, C.B., Qin, C.J., Wang, W.Q., Zhao, M.C., 2008. Stable isotopic compositions of the Hongshan skarn copper deposit in the Zhongdian area and its implication for the copper mineralization process. Acta Petrol. Sin. 24 (3), 480–488 (in Chinese with English abstract).
White, E.D., 1974. Diverse origins of hydrothermal ore fluids. Econ. Geol. 69 (6), 954–972.
Wu, H.Y., Zhang, L.C., Chen, Z.G., Wan, B., Xiang, P., Zhang, X.J., 2010. Hypersaline, high-oxygen fugacity and F-rich fluid inclusions in Jiguanshan porphyry molybdenum deposit, Xilamulun metallogenic belt. Acta Petrol. Sin. 26 (5), 1363–1374 (in Chinese with English abstract).

Wu, T.X., 2010. Geological characteristics and metallogenic model of Saishitang copper deposit in Qinghai Province. Min. Explor. 1 (2), 140–144 (in Chinese with English abstract).
Wu, Y.B., Zheng, Y.F., Gong, B., Zhao, Z.F., 2005. Zircon U–Pb ages and oxygen isotope compositions for granite at Xinkailing in the Beihuaiyang zone and their significance. Earth Sci. 30 (6), 659–672 (in Chinese with English abstract).
Xu, J.H., Xie, Y.L., Zhang, J.H., Jin, Y., Liu, Y.T., 2006. Sub-volcanic epithermal mineralization of Jiulongwan silver–polymetal deposit, eastern Daqingshan, Inner Mongolia, China: evidence from fluid inclusion. Acta Petrol. Sin. 22 (6), 1735–1743 (in Chinese with English abstract).
Yan, Z., Wang, Z.Q., Li, J.L., Xu, Z.Q., Deng, J.F., 2012. Tectonic settings and accretionary orogenesis of the West Qinling Terrane, northeastern margin of the Tibet Plateau. Acta Petrol. Sin. 28 (6), 1808–1828 (in Chinese with English abstract).
Zhai, D.G., Liu, J.J., Wang, J.P., Yang, Y.Q., Liu, X.W., Wang, G.W., Liu, Z.J., Wang, X.L., Zhang, Q.B., 2012. Characteristics of melt–fluid inclusions and sulfur isotopic compositions of the Hashitu molybdenum deposit, Inner Mongolia. Earth Sci. J. China Univ. Geosci. 37 (6), 1279–1290 (in Chinese with English abstract).
Zhang, D.H., 1997. Some new advances in ore-forming fluid geochemistry on boiling and mixing of fluids during the processes of hydrothermal deposits. Advance Earth Sci. 12 (6), 546–550 (in Chinese with English abstract).
Zhang, D.H., Xu, J.H., Yu, X.Q., Li, J.K., Mao, S.D., Wang, K.Q., Li, Y.Q., 2011. The diagenetic and metallogenic depth: main constraints and the estimation methods. Geol. Bull. China 30 (1), 112–125.
Zhang, F.W., Guo, A.L., Yao, A.P., 2004. Western Qinling–Songpan continental tectonic node in China's continental tectonics. Earth Sci. Front. 11 (3), 23–32 (in Chinese with English abstract).
Zhan, F.Y., Gu, F.B., Li, D.S., Gao, L.Q., Kui, M.J., 2007. Tectonic environment of adakite in eastern Kunlun area, Qinghai, and its ore-forming significance. Acta Geol. Sin. 81 (10), 1352–1368 (in Chinese with English abstract).
Zhang, G.W., Zhang, B.R., Yuan, X.C., Xiao, Q.H., 2001. Qinling Orogenic Belt and Continental Dynamics. Science Press, Beijing, pp. 1–855 (in Chinese).
Zhang, J., Qi, J.P., Qiu, J.J., You, S.N., Li, G.P., 2007. Compositional study on ore fluid of the Yindonggou silver deposit in Neixiang County, Henan Province, China. Acta Petrol. Sin. 23 (9), 2217–2226 (in Chinese with English abstract).
Zhang, L.G., 1985. The Application of the Stable Isotope to Geology, the Hydrothermal Mineralization of Metal Activation and It's Prospecting. Shaanxi Science and Technology Publishing House, Xi' an, pp. 1–267 (in Chinese).
Zhang, X.T., Yang, S.D., 2007. The Plate Tectonics of Qinghai Province—A Guide of the Geotectonic Map of Qinghai Province. Geological Publishing House, Beijing, pp. 1–221.
Zhang, Z.Y., Zhu, Y.T., 2001. Geological survey report of Xinghaifu region (1:250000). Qinghai Geological Survey Institute, pp. 1–464 unpublished (in Chinese).
Zheng, Y.F., Xu, B.L., Zhou, G.T., 2000. Geochemical studies of stable isotopes in minerals. Earth Sci. Front. Chin. Univ. Geosci., Beijing) 7 (2), 299–320 (in Chinese with English abstract).
Zhu, Y.F., Zeng, Y.S., Jiang, N., 2001. Geochemistry of the ore-forming fluids in gold deposits from the Taihang Mountains, northern China. Int. Geol. Rev. 43 (5), 457–473.
Zhu, X.Y., Zhang, Z.Y., Qi, W.X., 2012. Report on the Research Project of ore-Forming Rule and Model of the Saishitang Copper-Polymetallic ore Deposit of Qinghai Province. Beijing Institute of Geology for Mineral Resources, pp. 1–141 (in Chinese).